Myosin cross-bridge behaviour in contracting muscle – the T_1 curve of Huxley & Simmons (1971) revisited.

Carlo Knupp[1] and John M. Squire[2,3]

[1] School of Optometry and Vision Sciences, Cardiff University, Cardiff CF10 3NB, UK.
e-mail: knuppc@cardiff.ac.uk.
[2] Muscle Contraction Group, School of Physiology, Pharmacology & Neuroscience,
University of Bristol, Bristol BS8 1TD, UK. Email: j.m.squire@bristol.ac.uk
[3] Faculty of Medicine, Imperial College, London SW7 2BZ, UK. email: j.squire@imperial.ac.uk.

Correspondence: j.squire@imperial.ac.uk

Abstract: The stiffness of the myosin cross-bridges is a key factor in analysing possible scenarios to explain myosin head changes during force generation in active muscles. The seminal study of Huxley and Simmons (1971: *Nature* **233**: 533) suggested that most of the observed half-sarcomere instantaneous compliance (=1/stiffness) resides in the myosin heads. They showed with a so-called T_1 plot that, after a very fast release, the half-sarcomere tension reduced to zero after a step size of about 60Å (later with improved experiments reduced to 40Å). However, later X-ray diffraction studies showed that myosin and actin filaments themselves stretch slightly under tension, which means that most (at least two-thirds) of the half sarcomere compliance comes from the filaments and not from cross-bridges. Here we have used a different approach, namely to model the compliances in a virtual half sarcomere structure *in silico*. We confirm that the T_1 curve comes almost entirely from length changes in the myosin and actin filaments, because the calculated cross-bridge stiffness (probably greater than 0.4 pN/Å) is higher than previous studies have suggested. In the light of this, we present a plausible modified scenario to describe aspects of the myosin cross-bridge cycle in active muscle. In particular, we suggest that, apart from the filament compliances, most of the cross-bridge contribution to the instantaneous T_1 response comes from weakly-bound myosin heads, not myosin heads in strongly attached states. The strongly attached heads would still contribute to the T_1 curve, but only in a very minor way, with a stiffness that we postulate could be around 0.1 pN/Å, a value which would generate a working stroke close to 100 Å from the hydrolysis of one ATP molecule. The new program can serve as a tool to calculate sarcomere elastic properties for any vertebrate striated muscle once various parameters have been determined (e.g. tension, T_1 intercept, temperature, X-ray diffraction spacing results).

Keywords: myosin filament stiffness, actin filament stiffness, myosin cross-bridge stiffness, muscle transients, weak binding heads, contractile mechanism, cross-bridge cycle, rigor muscle

1. Introduction

Following the insight of A.F. Huxley [1] about the way force might be produced in muscle, Huxley and Simmons [2] carried out mechanical studies of frog muscle fibres subjected to rapid mechanical transients (shortening and lengthening) and found results which they thought the

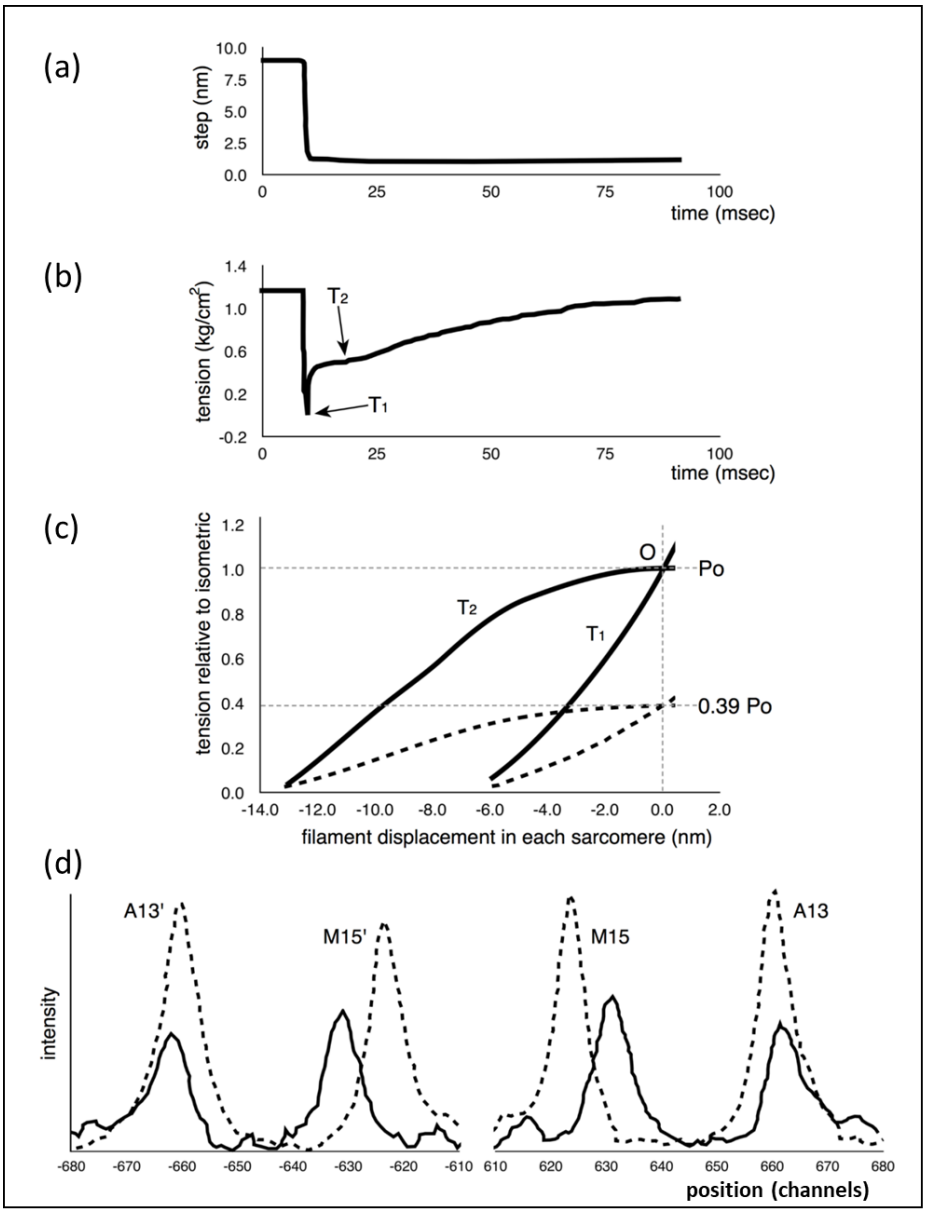

Figure 1: Previous observations: (a,b) Representation of the observations of Huxley and Simmons [2] (as improved by [3.4]) showing the tension transient (b) in an active frog muscle fibre after a rapid shortening step (a) of about 6 nm (60 Å) per half sarcomere and the point where the T_1 tension was recorded (b). (c) The T_1 and T_2 plots from experiments as in (a), but for different shortening steps (filament displacement per half sarcomere) and shown at two different sarcomere lengths – solid lines full overlap, dashed lines 3.1 μm. P_o is the isometric tension at the tension plateau. (d) Representation of the results from Huxley *et al* [5] showing the change in positions of the M15 (M15' on the opposite side) and A13 (A13') meridional X-ray diffraction peaks from myosin and actin filaments respectively at rest (solid lines) and full activation (dashed lines). The peaks shift towards the middle (longer spacings) and increase in intensity in X-ray patterns from active muscle. Wakabayashi *et al.* [6] obtained similar results. Figures redrawn from (a,b,c) [2] and (d)[6].

Huxley [1] scheme would not explain. What they did, for example, was to apply very rapid shortening steps, over within about 1.0 ms, to an active fibre (Figure 1(a)), reducing the muscle sarcomere length by various steps in the nm range, and then observing the tension recovery after each step. From these observations they plotted two curves. One was the tension level reached almost in synchrony with the applied length step (Fig. 1(b)). This was the so-called T_1 curve and was an expression of the instantaneous stiffness (or compliance = 1/stiffness) of the half-sarcomere. The other curve, the T_2 curve, related to the non-linear active recovery of tension for a few tens of ms after the step, a recovery directly attributed to force-generating myosin head cross-bridges interacting with actin. They tried to make the length step as fast as possible so that the recovery process, which would tend to reduce the apparent T_1 tension drop, was not too great during the step. This and other more recent studies with faster steps (Ford *et al*., 1977[3]; 1981[4]) concluded that most (>95%) of the instantaneous half sarcomere compliance resides in the myosin heads, not in the myosin or actin filaments. They also showed (Figure 1(c)) that their observed T_1 and T_2 curves appeared to scale directly with the amount of overlap between the myosin and actin filaments, a result which seemed to confirm that the T_1 and T_2 curves were solely revealing properties of independently acting, actin-attached myosin cross-bridges.

The new work of Ford *et al* [3,4] improved the observations by making the shortening steps much faster (0.2 ms instead of 1 ms) so that the recovery of tension as part of the T_2 curve was not too great during the initial step. Even though the recovery starts straight away during the step, the first part of the T_1 curve (i.e. for very small steps) is less affected by the tension recovery process and its slope can be extrapolated to the zero tension axis to give a more reliable value of the T_1 cutoff (they called this y_o). They also corrected their observed y_o value for inertia in the fibre and other factors (see [3,4]) to give a final value of around -4 nm. The results were modelled based on early analysis by Thorson and White [5].

This story was questioned by the results of H.E. Huxley *et al.* [6] and Wakabayashi *et al.* [7] (later by Brunello *et al*. [8]) who monitored the positions of three meridional peaks in observed X-ray diffraction patterns from frog muscle which was either relaxed, or fully active (tension P_o), or fully active and further stretched (extrapolated to tension $2P_o$). The reflections that they studied were the third order (M3) meridional peak from the myosin filaments of repeat 429 Å, the 15^{th} order meridional peak (M15) from the myosin filaments and the 13^{th} order meridional peak (A13) from the ~ 355 Å repeat of the actin filaments. They found (Fig. 1(d)) that the M15 (M15′) and A13 (A13′) peaks both shifted to longer spacings (towards the middle in Figure 1(d)) when the muscle carried full isometric tension (P_o). They also found that both peaks increased in intensity. Further, similar changes occurred when the active muscles were then stretched to give a tension equivalent to $2P_o$. These results showed that the myosin and actin filaments were themselves stretching and this meant that only part of the T_1 compliance observed by Huxley and Simmons [2] could be coming from the myosin cross-bridges.

More recent muscle mechanics experiments have also come to the conclusion that much of the compliance comes from the myosin and actin filaments and that the myosin cross-bridges must be relatively stiff. As reviewed by Offer and Ranatunga [9], Månsson *et al* [10], Kaya *et al*. ([11]; for single molecule results), and many references in those reviews, many studies suggested that the cross-bridges contribute only about one-third of the observed half sarcomere compliance. Often the cross-bridge stiffness was calculated by subtracting the observed filament stiffnesses from the total half-sarcomere stiffness. The resulting stiffness could then be shared among the attached

cross-bridges if the number of attached bridges was known. Offer and Ranatunga [9] discussed some of the dangers in these calculations, as has Månsson [12] who considered the effects of non-linearity in the sarcomere system. The results of Huxley and Simmons [2] were reconsidered by Huxley and Tideswell [13] in the light of the X-ray diffraction evidence for filament compliance and they claimed that the original Model [2] with some modifications could still be made to fit the observations. Reference [10] summarises some of these results and notes that the highest crossbridge stiffness reported in the literature is 4 pN/nm (or in our preferred units 0.4 pN/Å).

Analysis of recent X-ray diffraction data on the cross-bridge cycle [14] and results from protein crystallography [15] reveal a plausible cross-bridge cycle, but without discussing myosin head stiffness. Since the stiffness of the myosin cross-bridge is so fundamentally important for a proper understanding of the mechanism of contraction, we have now set up rigorous 'in silico' Models of the half sarcomere, including all the known stiffnesses. We have then subjected these Models to the different experiments described above. We found that the cross-bridges contribute even less to the half-sarcomere compliance than has been thought. The T_1 curves of Huxley and Simmons [2] are almost entirely explained by the behaviour of the myosin filament backbones and the actin filaments, and the cross-bridges contributing mainly to the T_1 curve are stiffer than has been suggested before. We discuss the new results in terms of a modified scenario for the myosin cross-bridge cycle in active muscle. In particular we suggest that almost all of the cross-bridge contribution to the T_1 curve comes from weakly-binding heads.

We note to start with that many of the observations that we are seeking to model have been recorded from different muscle types at different temperatures, so, for simplicity, we start the analysis assuming that all observations that we model apply to the same muscle type at the same temperature and then we demonstrate what would happen if this is not the case.

2. Materials and Methods

2.1 Setting up the 'in silico' Models.

We chose to set up several Models of ever-increasing complexity:

Model 1: This was a simple, approximate, purely theoretical, 1D Model of just a few stiffnesses in the system to test the effects of a stretch equal to the T_1 intercept at zero force on filament lengths.

Model 2: This was an exact calculation with a more detailed *in silico* mechanical Model than **Model** 1, but with a crosslink representing several myosin heads bridging to actin on every 143 Å crown repeat. In the program, 30% or 50% labelling was mimicked by weighting the head stiffness by a factor of 0.3 or 0.5.

Model 3: This was an exact calculation with a more sophisticated version of Model 2 in which the pattern of myosin head labelling of actin was modelled in 3D using a modified version of the MusLABEL program [16]. 20%, 30%, 50% or 100% labelling was determined in 3D by the cross-bridge search parameters in MusLABEL. Each half A-band component was also given a size and weight to allow X-ray diffraction results to be modelled.

2.2 Observations to be fitted:

These observations are amalgamated mainly from Ford *et al* [3,4]), Huxley *et al*. [6] and Wakabayashi *et al*. [7], although Brunello *et al* [8] have some analogous results. Note that the

myosin filament length changes by about 1% on activation [17,18], with changes due to tension generation being superimposed on this increase.

P_o: 480 pN per myosin filament (for frog *Rana temPoraria* at 2 ºC)
M3 Position rest: 143.2 Å (frog muscle)
M3 Position after activation (P = 0; ~1.0% change)): 144.9 Å
M3 Position after activation and with tension Po (~0.21% change): 145.2 Å
M3 intensity (active /rest): 1.4 to 2.0
A13 Position rest: 27.36 ± 0.01 Å
A13 Position active plateau (Po; ~0.3% change): 27.44 ± 0.01 Å
A13 Position active stretched (2Po): 27.49 ± 0.01 Å
M15 Position rest: 28.64 ± 0.01 Å
M15 Position after activation (P = 0; ~1.0% change)): 28.98 ± 0.01 Å
M15 Position active plateau (Po; ~0.21% change)): 29.04 ± 0.01 Å
M15 Position active stretched (2Po): 29.10 ± 0.01 Å
M15/A13 intensities at rest: 1.22 ± 0.06
M15 intensity active/rest: 1.79 ± 0.09
A13 intensity active/rest: 1.96 ± 0.10
T_1 intercept at zero force at full overlap: -40Å
M-region (half bare zone) length relaxed: 800 Å
M-region after activation (~1% change): 809.5 Å
M-region at active plateau (Po; ~0.21% change): 811 Å

It should be noted, as mentioned above, that these results are from a variety of muscles held at varying temperatures between about 0 and 14°C (see Appendix C). This means that any numerical values for stiffness that we obtain will need to be adjusted in a way that we detail later when all of the relevant experiments have been carried out on the same muscle type at the same temperature.

3. Results

In all our Models the stiffnesses of the myosin heads, and the actin and myosin filaments in the whole half sarcomere are all represented by Hookean springs. We do not make assumptions or guesses about what the tensions might be in different parts of the half sarcomere. The elastic properties of the whole assembly are calculated exactly from the spring constants. Throughout we discuss stiffnesses in units of pN/Å.

3.1 Preliminary analysis:

Before we get onto our realistic and exact *in silico* Models, we can consider a very simple approximate calculation. We know that the myosin filament spacing on average changes from 143.2 to 144.9 Å after the 1% activation increase and then to 145.2 Å (a change of 0.3 Å or 0.21%) under a force P_o of 480 pN. Assuming that the tension through the bridge region is equally distributed between actin and myosin filaments, with the average force on the myosin filament through the bridge region of about 0.5 P_o, then the myosin filament stiffness in the region between adjacent crowns is $\mathbf{k_m}$ = (0.5 x 480)/0.3 = 800 pN/Å. In a similar way, the actin filament A13 spacing

Preprints (www.preprints.org) | NOT PEER-REVIEWED | Posted: 14 March 2019 doi:10.20944/preprints201903.0147.v1

Peer-reviewed version available at Int. J. Mol. Sci. 2019, 20; doi:10.3390/ijms20194892

changes from 27.36 to 27.44 Å (i.e. 0.08 Å, a 0.3 % change) under an average force of 240 pN (there are two actin filaments for every myosin filament so the force is halved). Here the I-band part of actin will carry the full 240 pN force, but the overlap part will carry an average force of approximately 0.5 x 240 pN. So the actin filament stiffness between adjacent actin monomers is $\mathbf{k}_a$ = 240/0.08 = 3000 pN/Å for I-band actin and 120/0.08 = 1500 pN/Å for the overlap part of actin. These should be combined by the fact that the overlap is about 7114 Å long compared to 2844 Å in the I-band (see below). This is done by adding length-weighted reciprocals of the stiffnesses to give:

$$1/\mathbf{k}_a = [2844/(2844 + 7114)] / 1500 + [7114/(2844+7114)\ ] / 3000 = 1/2333 \text{ Å/pN}.$$

So the actin filament stiffness is roughly 2333 pN/Å.

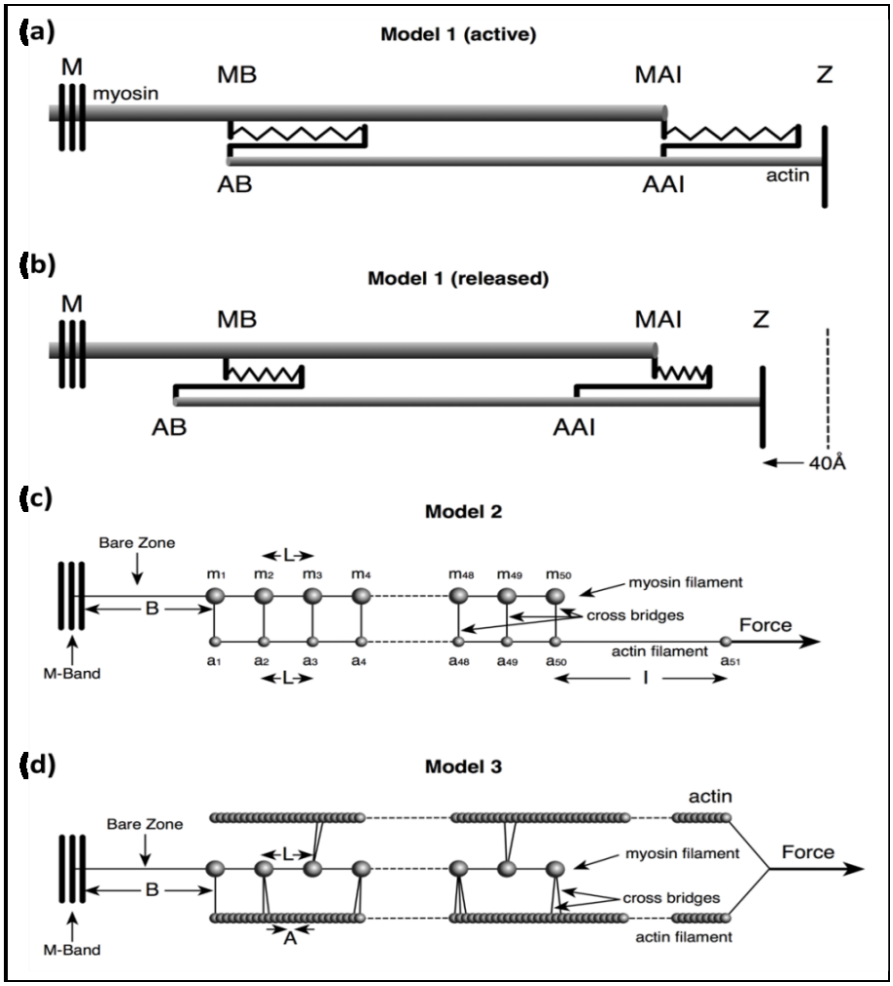

Figure 2: Illustrations of the three different Models of increasing complexity used in the calculations in this paper. (a,b) Model 1 allows a simple and approximate evaluation of filament and cross-bridge stiffnesses to show roughly what they must be. (MB; edge of the myosin filament bare zone; MAI the end of the myosin filament at the A-I junction; AB the tip of the actin filament away from the Z-band; AAI, the actin filament position at the A-I junction - all at the isometric force plateau before release.) (c) Model 2 mimics cross-bridges at levels m1, m2 etc attaching to actin positions a1, a2 etc at 144.9 Å intervals with appropriate weighting to allow for binding to actin by only a fraction of the available heads at any one time. (d) Model 3 represents in a simplified way the kind of result from assessing myosin head labelling realistically in 3D using the program MusLABEL [16]. For details see text.

3.2 Model 1:

In Model 1 active of Figure 2(a), simulating an isometric tetanus, the bare zone length (M to MB) in active muscle (force per myosin filament 480 pN) is taken as 811 Å, a 0.21% stretch from activated zero force of the M-region length of 809.5 Å. The myosin filament bridge region (MB to MAI) is 49*145.2 = 7115 Å long [19] and the actin filament (from AB to Z) is 364*27.44 = 9988 Å. The A-band part of actin (AB to AAI) is 7115 Å. The non-overlap part of the actin filaments in the I-band (AAI to Z) is 9988-7115 = 2873 Å. After a release to zero force through shortening of the half sarcomere by 40 Å (Fig. 2(b): Model 1 released), the half bare zone (M to MB) shortens by 0.21% from 811 Å to 809.5 Å (i.e. 1.5 Å), the bridge region shortens by 0.21% from 7115 Å to 7100 Å (i.e. 15 Å) and the actin filament from AAI to Z shortens by 0.3% from 2873 Å to 2864 Å (i.e. 9 Å). The overlap part of actin (AB to AAI) shortens from 7115 to 7094 Å (21 Å). In summary, MB moves towards the M-band by 1.5 Å, MAI moves towards MB by 15 Å, giving a total of 15 + 1.5 Å shift towards the M-band, AAI shifts towards the M-band by 40 Å less the shortening in that part of the thin filament (AAI to Z) by 9 Å, giving 31 Å, and AB moves towards the M-band by the 32 Å shift of AAI less the shrinkage of AB to AAI of 21 Å, a total of 11 Å.

In terms of cross-bridge movement, the bridge position at the M-region (bare zone) edge, assumed to be going from MB to AB, changes by 11- 1.5 = 9.5 Å. The bridge at MAI moves by the AAI shift of 31 Å less the MAI shift of 16.5 Å, a total of 14.5 Å. For, say, 30% attachment there would be 294 x 0.3 heads attached from one half myosin filament = 88 heads. These generate 480 pN of force or 480/88 = 5.45 pN per head. If we assume that heads throughout the overlap region behave in a similar way to those at the ends (MB and MAI) then the central average head will have changed length by (14.5 + 9.5)/2 = 12 Å. Applying the formula $F = \mathbf{k}_h \Delta x$ we can get the average value of the stiffness of one head $\mathbf{k}_h$ from $\mathbf{k}_h = F/\Delta x = 5.45/12 = 0.45$ pN/Å. For 20% attachment the force per head would be 480/(294 x 0.2) = 8.16 pN per head and the stiffness would be $\mathbf{k}_h = 8.16/12 =$ 0.68 pN/Å.

These are underestimates of $\mathbf{k}_h$ because, in fact, the overlap part of actin will stretch less than 0.3% and the I-band by more than 0.3% because of the head interactions with the actin filaments in the overlap region. So, in reality, the cross-bridge ends will not move as much as above and so their actual stiffness will be higher than we have calculated.

In other words, the calculations in Model 1 take no account of the effects of combining stiffnesses in the overlap region of the A-band. It is a very simplistic Model, but it defines a lower limit to the required T_1 cross-bridge stiffness value. In order to generate more realistic stiffness values, we tried our first *in silico* Model, Model 2.

3.3 Model 2:

In Model 2 (Figure 2(c)) the myosin filament backbone between every crown was a Hookean spring with stiffness $\mathbf{k}_m$. The myosin backbone was broken up into pieces (L =) 144.9 Å long for active muscle and the actin filament was also segmented to 144.9 Å lengths where myosin binding to actin is assumed to occur. Myosin crowns were numbered $\mathbf{m}_1$ to $\mathbf{m}_{50}$ (ignoring the missing crown towards the filament tip; Figure 2 Model 2**)** and likewise the 144.9 Å long A-band actin filament segments were numbered from $\mathbf{a}_1$ to $\mathbf{a}_{50}$. The I-band part of actin was assumed to be a single spring from $\mathbf{a}_{50}$ terminating at the Z-line at $\mathbf{a}_{51}$. $\mathbf{k}_a$ is the spring constant between actin monomers A = 27.36 Å apart axially, so the spring constant for the 144.9 Å segment of this single actin filament in the Model, which represented two actin filaments in the muscle, is $2*\mathbf{k}_a*A/L$. The

Preprints (www.preprints.org) | NOT PEER-REVIEWED | Posted: 14 March 2019 doi:10.20944/preprints201903.0147.v1

Peer-reviewed version available at Int. J. Mol. Sci. 2019, 20; doi:10.3390/ijms20194892

spring constant for a crown of heads is 6*Att*$\mathbf{k_h}$ where the Att value is the fraction of heads attached (e.g. 0.5 for 50% attachment). It is assumed that all the head springs are linear, obeying Hooke's Law, and are all the same. The spring constant of the bare zone (length B) is **bz** = (L/B)***km** and for the I-band (length I) is **ib** = 2*(A/I)*$\mathbf{k_a}$.

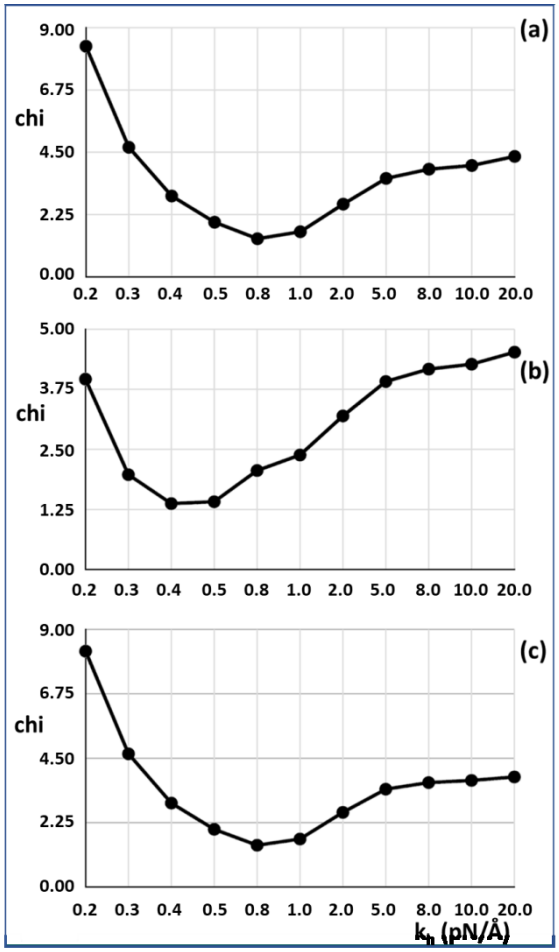

Figure 3: Results from Model 2 using optimised searching for good fits as measured by a goodness of fit factor Chi. The best results were obtained with a cross-bridge stiffness $\mathbf{k_h}$ around 0.45 to 0.8 pN/Å. (a) 30% attachment, (b) 50% attachment, (c) 30% attachment with the T_1 intercept unconstrained. In (a) and (b) the T_1 intercept was constrained to be 40 Å. In (c) the value of the T_1 intercept was unconstrained, but it still came out at around 40 Å. Note the non-linear scale for $\mathbf{k_h}$.

Appendix A shows the exact calculation required to find the positions of all the nodes in Model 2 after a force of 480 pN has been applied. What was done was to select a range of values of the cross-bridge stiffness from $\mathbf{k_h}$ = 0.2 to 20 pN/Å and then to do global searches to find the best fit to the observations on the A13 and M15 peak positions at $\mathbf{P_o}$ and 2$\mathbf{P_o}$ listed above. The calculated extended lengths of the myosin and actin filament ends were divided by the number of repeats so that the M15 and A13 spacings could be calculated.

In our modelling, the half sarcomere had a stretching force of $\mathbf{P_o}$ applied to see how it would extend, but in the reported experiments [2-4] the muscle had head-generated total force P_o and was

Preprints (www.preprints.org) | NOT PEER-REVIEWED | Posted: 14 March 2019 doi:10.20944/preprints201903.0147.v1

Peer-reviewed version available at Int. J. Mol. Sci. 2019, 20; doi:10.3390/ijms20194892

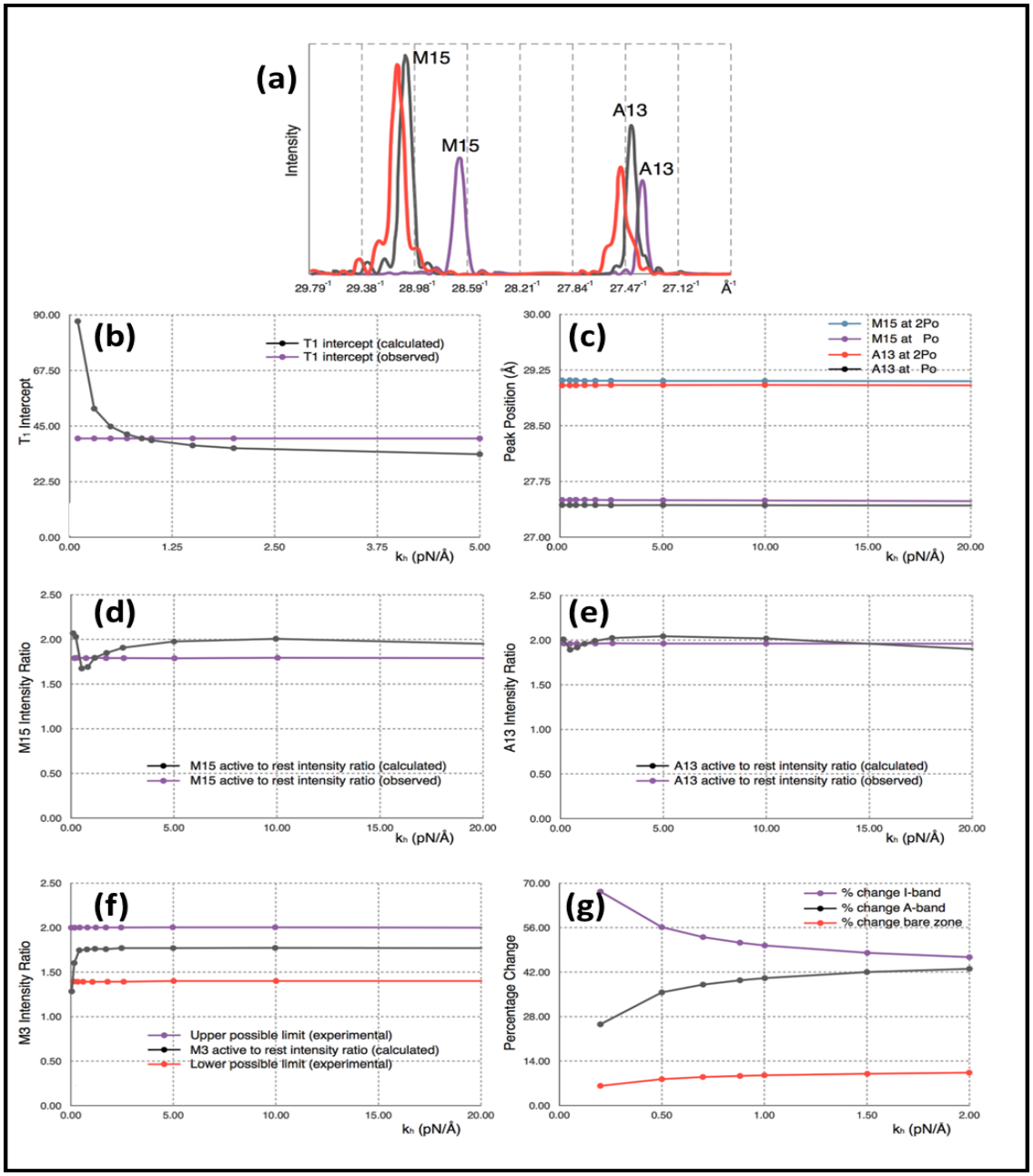

Figure 4: (a) Example of the computed X-ray profiles from calculations using Model 3. The purple curve is calculated from a resting muscle, the black curve from a muscle subject to a P_o = 480 pN external force and the red curve from a muscle subjected to a $2P_o$ external force. (b) Black curve: Changes of the T_1 intercept as a function of the head stiffness $\mathbf{k_h}$, with the filament stiffnesses held constant. Purple curve: observed value of the T_1 intercept (taken as 40Å). (c) M15 and A13 peak Positions as a function of head stiffness as calculated from the simulated X-ray diffraction from Model 3 after subjecting them to a P_o and $2P_o$ external force. (d) Black: M15 active to rest intensity ratio as a function of stiffness as calculated from Model 3; Purple - experimental measurement. (e) Black: A13 active to rest intensity ratio as a function of stiffness as calculated from Model 3; Purple - experimental measurement. (f) Black: M3 active to rest intensity ratio as a function of stiffness as calculated from Model 3; Purple: upper limit as found experimentally; Red: lower experimental limit. (g) Variation of the positions of various half sarcomere features as a function of head stiffness: Purple: I-band percentage change; Black: A-band percentage change and Red: bare zone percentage change.

then allowed to shorten. Since our Model is a purely elastic system, all stretches or releases are entirely reversible, so stretching an active half sarcomere by applying a force P_o is exactly the reverse of taking an activated sarcomere carrying force at P_o and allowing it to shorten to zero force. In other words, the actual experiments are equivalent in our Model to stretching it first by P_o, looking at the Positions of all the actin and myosin repeats, and then taking the load off to see what happens. The results for 30% attachment are shown in Figure 3(a,c). The best fit (lowest Chi value) without including the T_1 intercept as a constraint is at $\mathbf{k_h}$ = 0.8 pN/Å and the T_1 intercept is 39.47Å, almost exactly as observed (40 Å). For 50% attachment the best Chi is at $\mathbf{k_h}$ between 0.4 and 0.5 pN/Å and the T_1 intercept is also at around 40 Å (Figure 3(b)). The myosin and actin filament stiffnesses $\mathbf{k_m}$ and $\mathbf{k_a}$ were 720 and 2280 pN/Å respectively. So, at their face value, the Huxley and Simmons [2] and Ford *et al* [3,4] results are quite compatible with the X-ray results of Huxley *et al.* [6] and Wakabayashi *et al.* [7].

This is a much better Model than has ever been used before, but it still does not represent a realistic simulation of the pattern of cross-bridge labelling that occurs in the overlap region in 3D when myosin heads bind to actin. Our next Model, Model 3, uses our full knowledge of A-band symmetry.

3.4 Model 3:

Our most sophisticated Model used a modified version of MusLABEL [16] to find the best sites on actin for labelling on the six actin filaments surrounding a myosin filament. The A-band was assumed for simplicity to have the simple lattice structure found in bony fish muscle [18]. The labelling was then reduced down to that on two non-equivalent actin filaments (see Appendix B) as in an actual muscle. The program also calculated the meridional diffraction pattern from the whole assembly, particularly the A13, M15 and M3 reflections. The transforms were calculated by simply putting spheres in the correct Positions and weighting the spheres appropriately. We were not trying to simulate a full 2D diffraction pattern. In Model 3 (Figure 2), each myosin filament was assumed to be a series of 49 equal springs, spaced 144.9Å apart (the inter-crown spacing of the myosin filament cross-bridge array [17-20]) on the end of a single spring representing the half bare zone of the filament. Alongside the myosin filament were six helical actin filaments of subunit axial translation 27.36Å between successive actin monomers. The actin filaments lie along the bridge region of the myosin filaments and continue through the I-band to the Z-band, a total of 365 monomers. Every adjacent pair of actin monomers was linked by a spring of stiffness $\mathbf{k_a}$. Where the myosin and actin filaments overlap, and where MusLABEL showed heads could attach to actin, there were (axially aligned) springs between myosin and actin representing the stiffnesses of those attached heads.

Simulated 1D X-ray diffraction patterns (e.g. Figure 4(a)) were computed from the Model with each myosin cross-bridge or actin monomer represented as a sphere. The appropriately weighted sphere densities were projected onto the fibre axis and their contributions summed to give a 1D density profile from which the meridional Fourier transform was calculated. Individual sphere radii and weights were definable for: (i) detached heads in resting muscle, (ii) detached heads in active muscle (off and weak-binding heads), (iii) heads attached to actin in active muscle (strong binding heads), (iv) a myosin filament backbone component (assumed the same for relaxed and active muscle apart from the 1% change in axial spacing on activation) and (v) the actin monomers.

We note that there is some uncertainty about the contribution to the observed X-ray peaks from the actin filaments in the I-band part of the sarcomere. I-band actin is relatively disordered compared to A-band actin which is confined by the hexagonal myosin filament lattice [21]. There is also a transition of the actin filament positions from the square lattice at the Z-band to the hexagonal A-band array, so that in the I-band the actin filaments are not strictly parallel [22]. However, we obtained good results assuming that all the actin monomers throughout the half sarcomere contribute equally to the axial diffraction pattern. In all cases the effects of the compliance of the actin filaments in the I-band was always included in assessing the elastic properties of the sarcomere.

3.5 Model 3: Fitting the peak Positions and intensity increases

By exploration of parameter space we were able to come up with reasonable Models for the X-ray observations of Huxley *et al.* [6] and Wakabayashi *et al.* [7] as shown in Figure 4(a). In Table 1, parameters from the calculated diffraction pattern on the meridian close to the M15 and A13 peaks and at M3 from Model 3 are compared with the experimental values quoted above.

Table 1: Observed and Calculated X-ray values	30% attachment	**30% attachment**
	Observed	Calculated
A13 Position at rest (Å)	27.36 ±0.01	27.36
A13 Position at P_o (Å)	27.44 ±0.01	27.42
A13 Position at $2P_o$ (Å)	27.49 ±0.01	27.50
M15 Position at rest (Å)	28.64 ±0.01	28.64
M15 Position at P_o (Å)	29.04 ±0.01	29.05
M15 Position at $2P_o$ (Å)	29.10 ±0.01	29.11
Intensity M15rest / A13rest	1.22 ±0.06	1.25
Intensity M15active P_o / M15rest	1.79 ±0.06	1.63
Intensity A13active P_o / A13rest	1.96 ±0.06	1.91
Intensity M3active P_o / M3rest	1.4 to 2.0	1.96
T_1 x cutoff for zero tension	-40Å	-40.01Å

The explanation for the results is as follows. Firstly, the positions of the myosin M15 and actin A13 peaks in the simulation of active muscle are almost solely dependent on the force applied (P_o) and the values that we have used for the elastic constants of the myosin and actin filaments ($\mathbf{k_m}$ and $\mathbf{k_a}$). These peak positions do not depend appreciably on the head stiffness ($\mathbf{k_h}$). This can be seen in the plot in Figure 4(c) which shows M13 and A13 peak positions for active muscle plotted against the value of the head stiffness included in the calculations in the range 0.2 to 20 pN/Å, while the filament stiffnesses $\mathbf{k_m}$ and $\mathbf{k_a}$ were held at 720 and 2280 pN/Å. The intensity change of the M3 peak active/relaxed is also insensitive to $\mathbf{k_h}$ above about $\mathbf{k_h}$ = 0.25 pN/Å. Note that, in the examples shown, the attachment number is 30%, which is thought to be a reasonable value for the strong

binding heads [14,23,24], although reasonable results could be obtained for a range of attachments (e.g. 20 to 50%).

The intensity increases in the M3, A13 and M15 peaks arise as follows. The M3 and M15 intensities go up because we have modelled the detached heads in active muscle (including weak binding heads) as having a stronger contribution (i.e. their mass is axially sharper) than the detached heads in resting muscle [14]. The actin-attached heads also contribute to the active M15.

The actin A13 peak becomes stronger because of the labelling of actin by myosin heads in active muscle. For this strong A13 increase to occur, the diffraction from the attached heads needs to be quite well in phase with (i.e. at the same axial positions as) the diffraction from the actin monomers, although some increase in A13 may also be due to straightening of the actin filaments in the I-band when the muscle generates tension.

It should be noted here that the X-ray intensity Modelling was not definitive. Several combinations of parameters could fit the observations since there were many more free parameters to fit than the number of observations, a problem that we have discussed fully elsewhere [23,25]. The results presented here are simply to show that fitting the observed intensity changes in the M15 and A13 peaks is not a problem, even using simple spheres, given the assumptions above about the different head contributions. The choice of parameters to model the X-ray intensities here was not affected at all by the elasticity parameters used to model the observed quick release experiments. It is only the Positions of the X-ray peaks that tell us about the elastic properties of the filaments, and, happily, modelling these used more observations than parameters. Including the detailed head shape to calculate X-ray intensities is unnecessary and inappropriate in these calculations, where the resolution involved is low (around 30 Å) and there are far more parameters to fit than there are observations [25]. It is sufficient here to show that the observed intensities can be modelled sensibly, even if there are several ways of doing it.

3.6 Model 3: The elastic properties of the sarcomere

Having defined a Model which appears to satisfy all the X-ray diffraction criteria, we looked at the mechanical properties of this Model. Firstly we plotted the equivalents of the Huxley and Simmons [2] T_1 curves (Figure 5(a,b)) and compared these with the observations (Figure 5(c)) of Ford *et al*. [3,4]. Since the Model consists entirely of linear springs, the computed sarcomere behaviour is exactly linear. Figure 5(a,b) show what happens if the tension in our Model 3 half sarcomere starting at P_0 is allowed to drop to zero. There is a cut-off on the **x** axis (half sarcomere displacement) of around -40 Å, almost exactly what Ford *et al*. [4] measured. In fact they reported values between about -36 and -40 Å (Figure 5(c)), so there is some uncertainty in this observation. Despite this, the modelling confirms that the Huxley-Simmons [2] and Ford *et al* [4] results and the X-ray spacing measurements [6,7] are compatible.

Preprints (www.preprints.org) | NOT PEER-REVIEWED | Posted: 14 March 2019 doi:10.20944/preprints201903.0147.v1

Peer-reviewed version available at Int. J. Mol. Sci. 2019, 20; doi:10.3390/ijms20194892

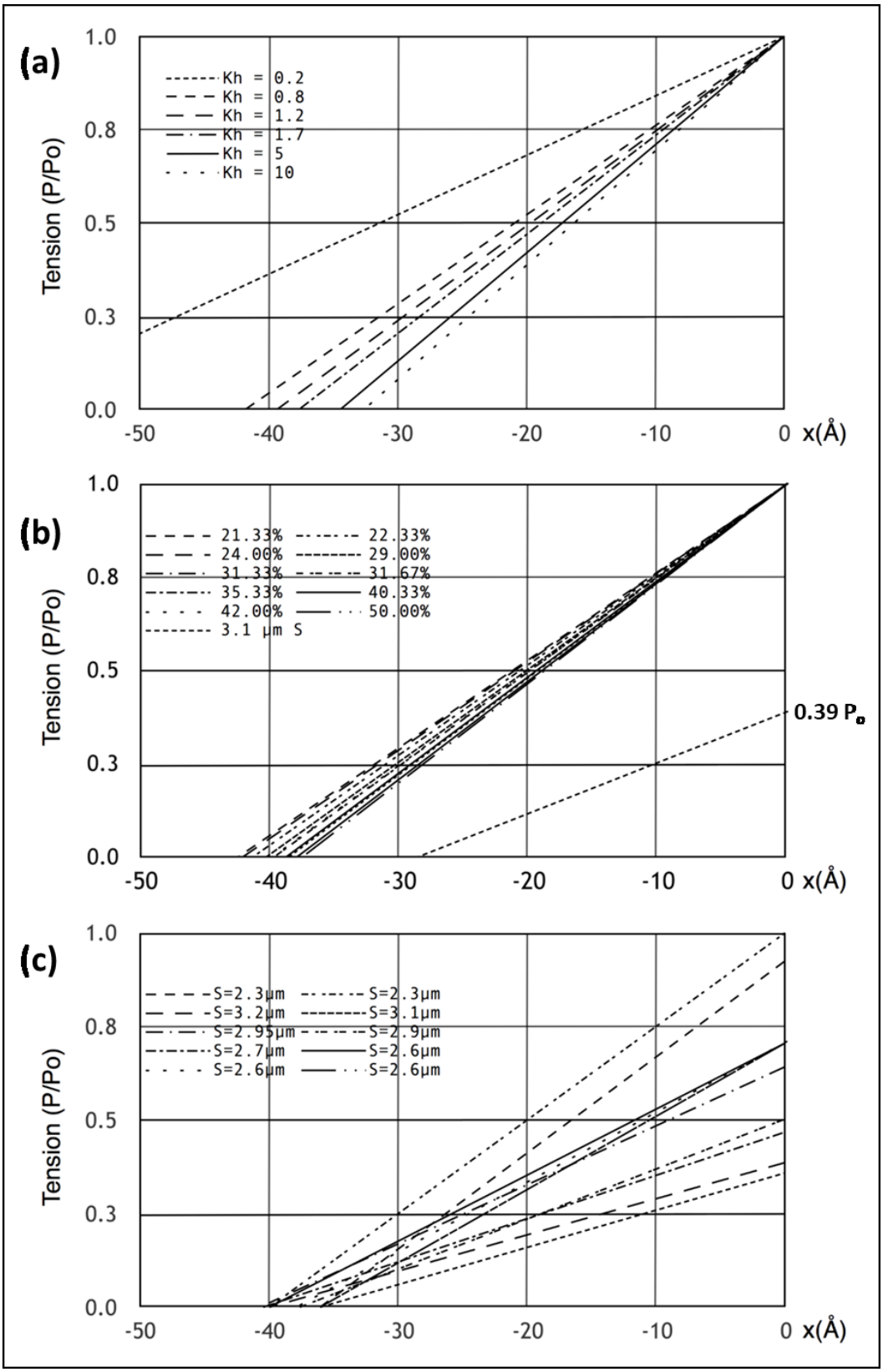

Figure 5: (a) T_1 plots showing the position of the T_1 intercept on the x axis for zero tension as a function of the myosin head stiffness in Model 3 for a muscle at full overlap. (b) Similar to (a) but here for different percentage cross-bridge attachments to actin at full overlap and also what happens at 3.1 µm sarcomere length (tension 0.39 P_o) using Model 3. (c) The observations of Ford *et al* [4] plotted here assuming purely linear elasticities and assuming that tension varies linearly with overlap, shown for comparison with (a) and (b).

Figure 5(a) shows the computed T_1 plots using the same parameters throughout apart from the value of the head stiffness $\mathbf{k_h}$ which was varied from 0.2 to 10 pN/Å (still using the same $\mathbf{k_m}$ and $\mathbf{k_a}$ values). The plots are very similar, except around $\mathbf{k_h}$ = 0.2 pN/Å. It is evident that there is only marginal information about the head stiffness in the T_1 plots if $\mathbf{k_h}$ is around 0.4 pN/Å or higher. Secondly, the T_1 plot depends very little on the number of attached heads. Figure 5(b) shows T_1 plots computed with $\mathbf{k_h}$ = 1 pN/Å for different numbers of attached heads, 21 to 50%. Once again, although there are small changes, the T_1 plots depend rather little on the number of heads attached.

Another key observation of the A.F. Huxley laboratory was the scaling of T_1 with the amount of overlap [4,26]. Ford *et al*. [4] carried out length step experiments over a range of sarcomere lengths in addition to their original measurement at S = 2.2 μm (Fig. 5(c); cf. Fig. 1(c)). We therefore set the sarcomere length to 3.1 μm, adjusted the tension to 0.39Po, assuming a linear tension drop from S = 2.2 μm to S = 3.6 μm, and carried out the same computations as before with the same parameters. The result is shown by the line from $0.39P_o$ in Figure 5(b). The plot is not perfect (the x cut-off is at -35 Å instead of -40 Å for a sarcomere length of S = 3.1 μm), but is not unlike the observations. There is variation down to 35 Å (Figure 5(c)) in the results of Ford *et al* [4]; variation that is very similar to the variations in Figure 5(a) and (b). However, our modelled fit can be made closer to 40 Å if titin is included as a linear spring that comes into play at longer sarcomere lengths. For example, with titin represented as a single elastic element from the myosin filament tip to the Z–band, a titin spring constant of 0.5 pN/Å starting at a sarcomere length of 3.0 microns gave a T_1 cut-off at S = 3.1 μm of exactly 40 Å. These parameters should not be taken too literally because there is uncertainty about the exact sarcomere length at which the titin elasticity comes into play and the effective titin filament stiffness is also unknown. But it illustrates the principle that titin could modify what happens to the T_1 plot at longer sarcomere lengths where the resting tension increases.

In a previous paper [23] it was estimated that the populations of the resting (off), weak binding and strong heads in fully active fish muscle were 48% off, 20% weak, 32% strong. In assessing cross-bridge stiffness this is important in that Brenner *et al* [27] (and references therein) showed that weak binding heads contribute strongly to half sarcomere stiffness in a length step complete in 0.2 ms. If similar weak binding bridges occur in active muscle, as we expect, then what is observed in relatively fast length step experiments such as those by Ford *et al*. [4] is likely to be due to the effects of both strong binding and weak binding heads. If the length steps are faster than this then the weak binding heads will probably contribute even more. We have therefore looked at the cross-bridge stiffness results for both 30% (strong only) and 20% (weak only) attachment. The result is that, in this Model, which is more sophisticated than any other Model which has been published previously, if the zero tension cut-off in the T_1 plot is taken to be exactly 40 Å, then the best value of $\mathbf{k_h}$ for 30% of the heads contributing to stiffness (strong states) is $\mathbf{k_h}$ = 0.88 pN/ Å and for 50% of the heads contributing (weak plus strong, assumed to have the same stiffness) is about $\mathbf{k_h}$ = 0.53 pN/ Å, much higher than has been thought before, but similar to the results from Models 1 and 2. We discuss the possible effects of weak-binding heads more fully later.

3.7 Model 3: Which parts of the sarcomere are stiff?

In order to understand our modelling we followed the positions of various actin monomers and myosin crowns as the sarcomere shortens during a T_1 plot. Key actin positions are the first and last overlapped actins in the A-band (**a1** and **a260** in Figure 2) and the first and last myosin crowns (**m1** and **m50** in Figure 2). The movements of these points during the T_1 plot (from tension = $\mathbf{P_o}$ to

Preprints (www.preprints.org) | NOT PEER-REVIEWED | Posted: 14 March 2019 doi:10.20944/preprints201903.0147.v1

Peer-reviewed version available at Int. J. Mol. Sci. 2019, 20; doi:10.3390/ijms20194892

zero) are shown in Figure 4(g) as a function of the head stiffness $\mathbf{k_h}$. It can be seen there that, for a $\mathbf{k_h}$ value around 0.5 to 1.0 pN/Å, the vast majority (about 50%) of the shortening is taking place in the I-band, between **a260** and the Z-band. Most of the rest of the shortening (about 40%) takes place in the overlap region and 10% in the M-region (bare zone). These values are not greatly affected by the stiffness of the myosin heads above about $\mathbf{k_h}$ = 0.5 pN/Å. The reason for this result appears to be that the cross-linked A-band system is relatively very stiff. The M-region extends so much (10%) because it experiences the full force P_o, whereas, on average, in the A-band, the force on the actin-linked myosin filament is about $0.5P_o$; most of the myosin filament cross-bridge region shortens by much less than the M-region. Even though at a sarcomere length of 2.2 μm the A-band represents 70% of the sarcomere length, only 40% of the shortening is taking place there; 50% of the shortening occurs in the relatively short I-band, only 25% of the sarcomere length.

3.8 Model 3: How do the cross-bridge stiffness or T_1 cut-off vary with P_o and other factors?

We mentioned earlier that many of the observations that we are fitting have come from different muscles at different temperatures (Appendix C). Since the MusLABEL program gives an exact calculation once the parameters are set up, it is very easy to test what would happen if, for example, the P_o value that we are using was different, or the T_1 cut-off at zero tension was different. In the following examples we have first assumed that the measurements of spacing changes of the M15 and A13 X-ray reflections are correct and have varied other parameters to see what happens.

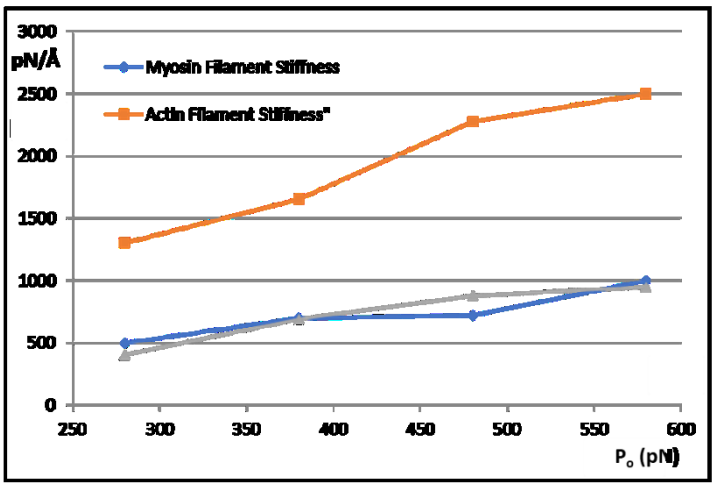

.

Figure 6: The variation of myosin ($\mathbf{k_m}$) and actin filament stiffnesses ($\mathbf{k_a}$) with tension P_o assuming that the X-ray spacing changes in the M15 and A13 peaks are as observed by Huxley *et al* [5] and Wakabayashi *et al* [6].

The results are shown in Figures 6 and 7. Figure 6 shows how the actin and myosin filament stiffnesses would change if the observed X-ray spacings apply, but the P_o value should be different. Figure 7(a) shows for 20% labelling that the T_1 cutoff and cross-bridge stiffness $\mathbf{k_h}$ follow closely spaced curves as P_o is varied from 280 to 580 pN. Figure 7(b) shows a similar trend for 30% labelling. So, assuming that in the Huxley and Simmons and Ford *et al* experiments, the T_1 cut-off on the x axis is at least somewhere near to 40 Å, and that the X-ray spacing measurements in Table 1 are reasonably accurate, the P_o tension level in our assumptions can be as low as, say, 300 pN, rather than 480 pN that we have used, and the cross-bridge stiffness would still be above 0.4 pN/Å;

higher than previously estimated. In addition Figure 7(c) shows a plot of P_o against k_h for a T_1 cut-off at 40 Å and different percentage attachments. In principle, if the experiments were all done on the same muscle at the same temperature, the parameter values obtained could be checked against Figures like Figure 7 to read off the appropriate cross-bridge stiffness.

Finally, if the X-ray spacing changes for known P_o values were measured to be different from those listed earlier [5,6], and therefore different from what we have assumed throughout in our calculations, then we could plug the new X-ray spacings directly into our MusLABEL program and directly calculate the cross-bridge stiffness as a function of T_1 intercept for these new X-ray values.

4. Discussion

4.1 Summary of results

In summary, we have shown with our *in silico* half sarcomere Models and exact calculations, particularly Model 3, which all give similar results: (1) that the observations of Huxley and Simmons [2], Ford *et al* [3,4], Huxley *et al.* [6] and Wakabayashi *et al.* [7] can be modelled directly (Figures 3,4 and 5), (2) that the myosin cross-bridges contributing to the T_1 curve seem to be stiffer than has been thought previously, but they are still locally very compliant relative to the local compliances of the myosin and actin filaments (Figures 3 and 7), (3) that the Huxley-Simmons [2] T_1 curves depend less than expected on cross-bridge stiffness (Figures 4(b), 5(a)), but they can be modelled using the known filament stiffnesses and with the same parameters that explain the X-ray observations in (1), (4) that the half sarcomere stiffness depends less than expected on the number of heads attached to actin (Figure 5(b)). However, the X-ray results fit well to an attachment number of heads of around 20 to 30%, (5) that the Huxley-Simmons T_1 curves and those of Ford *et al* [4] do scale reasonably well with the amount of filament overlap as the sarcomere length is changed (Figure 5(b)), as observed in their later studies, particularly if titin elasticity is included, but the myosin head compliance only makes a small contribution to this; it is filament compliance that is being seen. The reason for this seems to be that, as the sarcomere is extended, more and more of the relatively compliant I-band is being exposed (see Figure 4(g)), so the half-sarcomere compliance in non-linear.

Note that the relatively slow T_2 curves of Huxley and Simmons [2] are presumably, as they suggested, reporting the recovery behaviour of the myosin heads that are attached to actin in strong states where force is produced (Figure 1(b,c)). We discuss the T_2 curve elsewhere.

4.2 Head stiffness in rigor muscle

In work reported in 2014 [8], Brunello *et al* imposed small amplitude sinusoidal length oscillations on frog muscle fibres in rigor and measured the resulting tension changes (see Figure 8(b)). They obtained a length oscillation amplitude of around 28 Å peak to peak with a resulting tension change of around 193 kN m^{-2} (our estimates from their figure). We make this to be about 355 pN per myosin filament and two actins. This gives a half sarcomere stiffness per myosin and two actins of 12.6 pN/Å.

Using Model 3 we carried out the same procedure *in silico* to find out what cross-bridge stiffness would be needed to generate the observed rigor tension change assuming that the filament stiffnesses are as determined above to explain the M15 and A13 changes in position (Table 1). The result is that the cross-bridge stiffness needed to generate 355 pN of force with 100% labelling in Model 3 for a length change of 28 Å is 0.44 pN/Å. Brunello *et al*. [25], using a conventional method

of calculation, estimated the same stiffness to be 0.263 pN/Å, underestimating the myosin head stiffness based on our analysis.

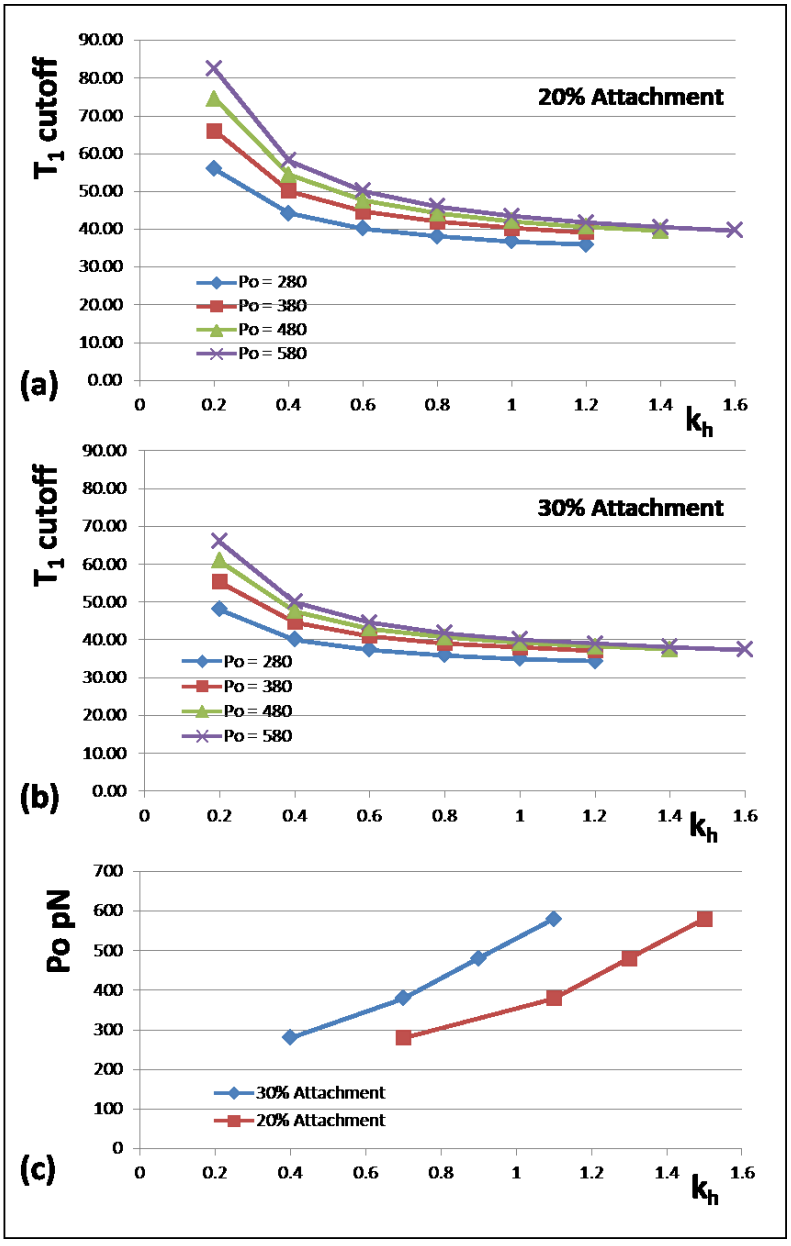

Figure 7: The variation of the T_1 intercept at zero force plotted against head stiffness (k_h) for different percentages of heads attached to actin (a) 20% and (b) 30% and at different P_o values (pN). (c) A plot of P_o against k_h for a T_1 cut-off at 40 Å and different percentage attachments. Throughout it is assumed that the changes in X-ray spacings shown in Figure 1(d) apply.

Preprints (www.preprints.org) | NOT PEER-REVIEWED | Posted: 14 March 2019 doi:10.20944/preprints201903.0147.v1

Peer-reviewed version available at Int. J. Mol. Sci. 2019, 20; doi:10.3390/ijms20194892

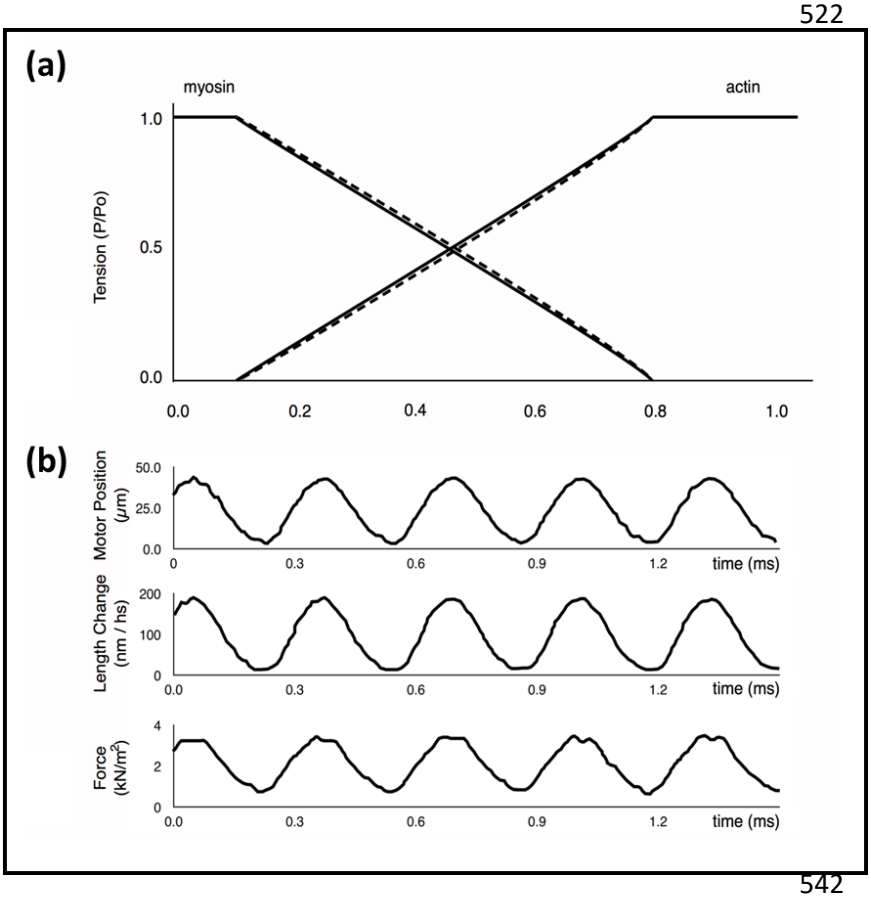

Figure 8: (a) Tension curves along the myosin and actin filaments as described in ref [24]. (b) Length and force response of rigor frog muscle fibres in experiments in [8]. (a) redrawn from [8] and (b) redrawn from [24].

4.3 Tension variations through the overlap region of the A-band

In many studies [3,4] it has been assumed that in active muscle the tension variation along the overlap region of the sarcomere is linear such that the tension in the myosin filament drops from P_o at the M-region edge, to $P_o/2$ half way along the bridge region, to zero at the filament tip [5]. Similarly, tension in each of the two non-equivalent actin filaments was assumed to increase linearly from zero at the bare zone edge (at full overlap) up to $0.5P_o$ at the A-band tip (A/I junction). We assumed this in our discussion of Model 1. This is graphically illustrated in a figure from Linari *et al* [24] redrawn here as Figure 8(a), where the force in the two actin filaments per myosin filament has been combined. This is the underlying assumption on which most previous estimates of sarcomere stiffness have been based [5].

However, the Model 2 program or the Model 3 MusLABEL program can be used to reveal directly the tension variations in the overlap region. In fact the tension variation is far from linear (Figures 9 and 10). Examples using Models 2 and 3 for different percentages of labelling are shown in Figure 9(a,b). The tension along the filaments shows the general trend as in Figure 8(a). But, as well as some local fluctuations which may not be surprising, there are marked periodic long period oscillations superimposed on this trend, with amplitude depending on the percentage attachment.

Since there can be slightly different ways of generating a given attachment number in MusLABEL, Figure 10 shows results similar to Figure 9, but averaged over a number of possible configurations. Exactly the same trends are evident for (a) 100% labelling and (b) 50% labelling.

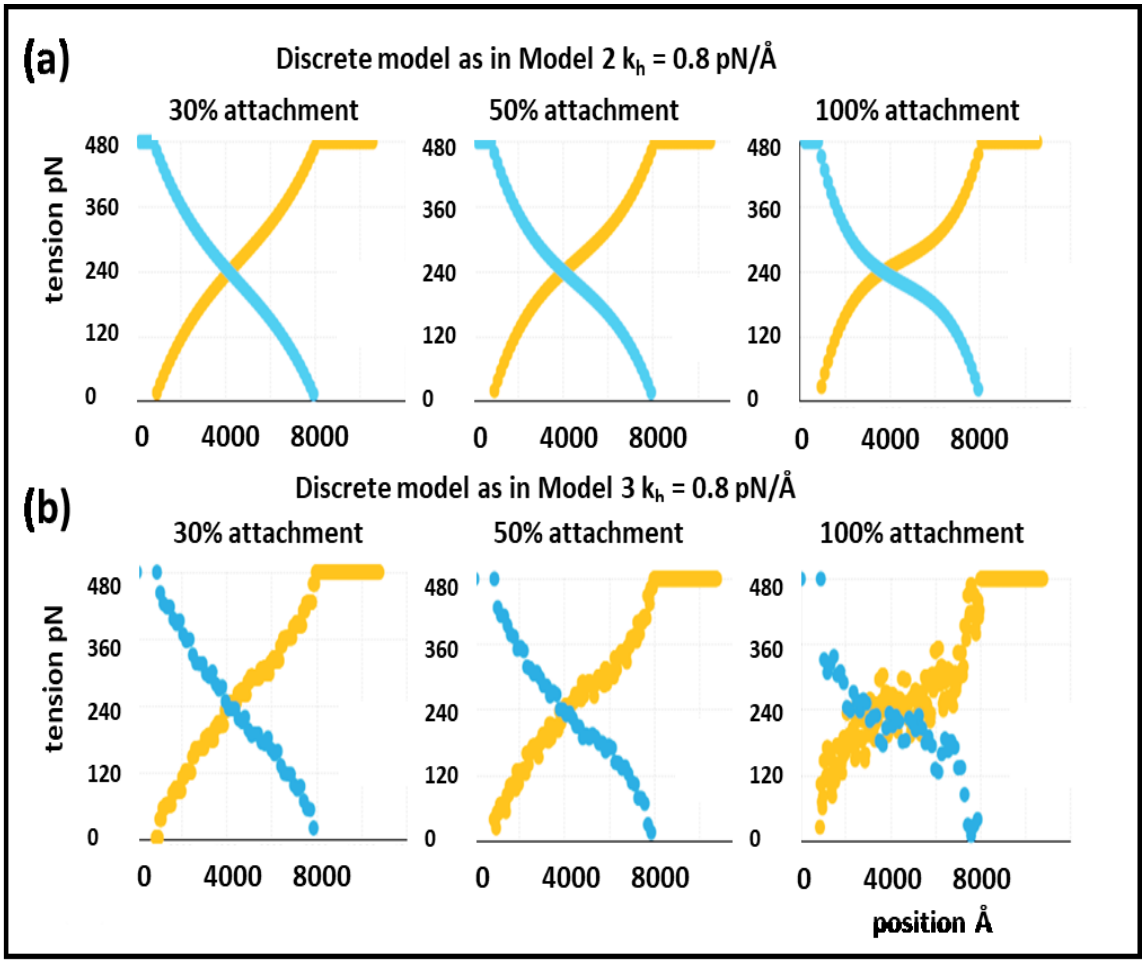

Figure 9: Tension curves along the myosin filament (blue) and actin filaments (orange) calculated from (a) Model 2 and (b) Model (3). The tension curves were calculated with 30% head attachment (first column), 50% head attachment (middle column) and 100% head attachment (third column). After applying a force of 480 pN to the last monomer in the actin filament and calculating the new monomer positions, we obtained the tension of the springs between adjacent monomers using Hooke's law, and we plotted these values as a function of spring's Position along the half-sarcomere. The position 0 corresponds to the centre of the M-band. In all cases $\mathbf{k_m}$ = 720 pN/Å for the myosin filament, $\mathbf{k_a}$ = 2280 pN/Å for the actin filament and $\mathbf{k_h}$ = 0.8 pN/Å for the heads. Note that the analysis of Ford *et al* [4] went part way towards this in their Figure 4 (lower left).

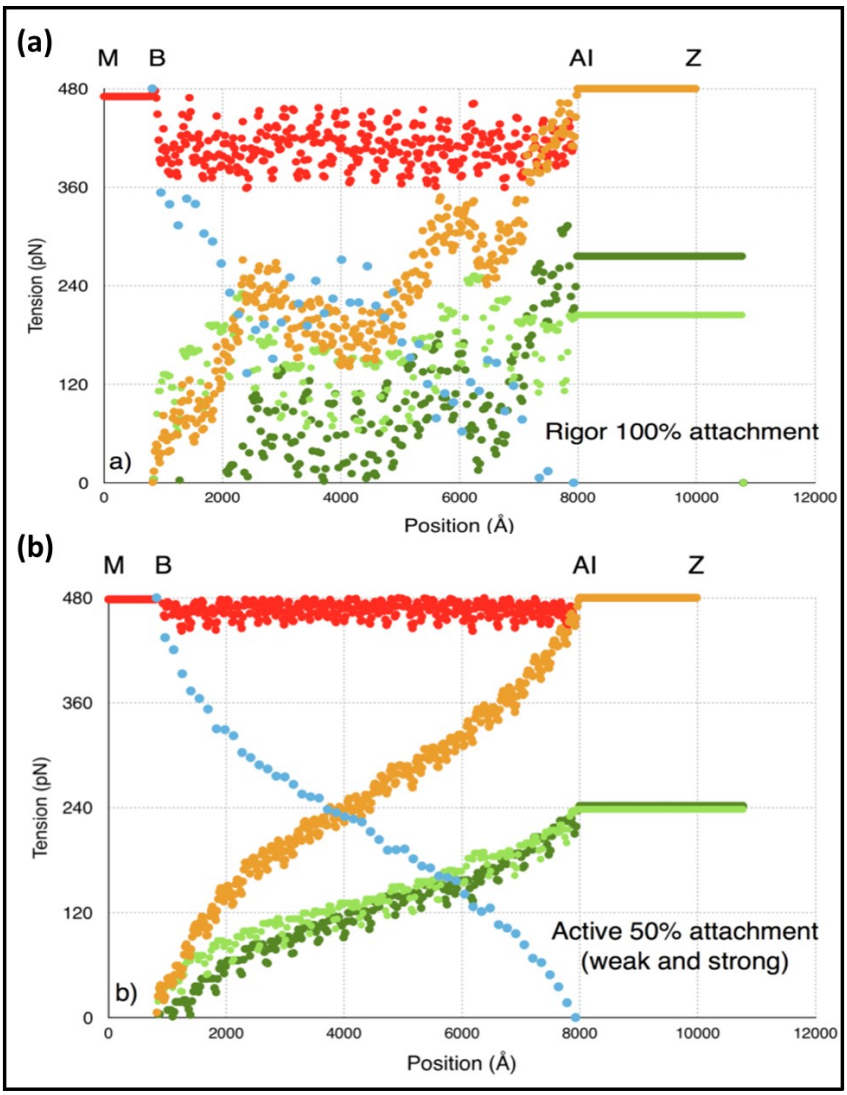

Figure 10: Tension through the half sarcomere, averaged over several possible initial configurations, using Model 3 for (a) 100% attachment and (b) 50% attachment. The tension along the myosin filament is depicted in blue, along one set of equivalent actins in light green and along the other set of equivalent actins in dark green. Their sum, corresponding to the tension along all actins, is depicted in orange. The summed tensions (actin plus myosin) along the A-band are depicted in red. In both cases $\mathbf{k_m}$ = 720 pN/Å for the myosin filament, $\mathbf{k_a}$ = 2280 pN/Å for the actin filament and $\mathbf{k_h}$ = 0.8 pN/Å for the heads.

4.4 Modelling Previous Studies of Cross-bridge Stiffness.

To investigate further why our results are different from previous estimates of cross-bridge stiffness and how the tension actually changes along the myosin and actin filaments, we built a new Model similar to that described in [4,5]. That original Model, used to derive an analytical description of the tension curves through the overlap region, assumed a continuous interaction between myosin and actin filaments via the myosin heads which were defined by their stiffness per unit length. This represented the cross-bridges as being like an elastic (rubber) sheet between the actin and myosin filaments, which sheared when the filament overlap changed. We mimicked this by having linear (cross-bridge) springs set very close together (10 Å apart). Our new Model

consisted of two series of monomers interconnected with springs with appropriate stiffness (Figure 11(a)). One series represented the myosin filament, the other the actin filament. The rest length L between the monomers in both filaments was set to 10 Å. The stiffness for the springs connecting the myosin monomers was set to K_m = 720 x 144.9 pN/Å, while for the springs between actin monomers it was K_a = 2 x 2280 x 27.36 (144.9 Å is the myosin periodicity in active muscles; 27.36 Å the actin periodicity; 720 pN/Å and 2280 pN/Å are stiffness values for myosin 144.9 Å repeat and the actin 27.36 Å repeat obtained above; the factor 2 for **K_a** indicates that there are two actin filaments for each myosin).

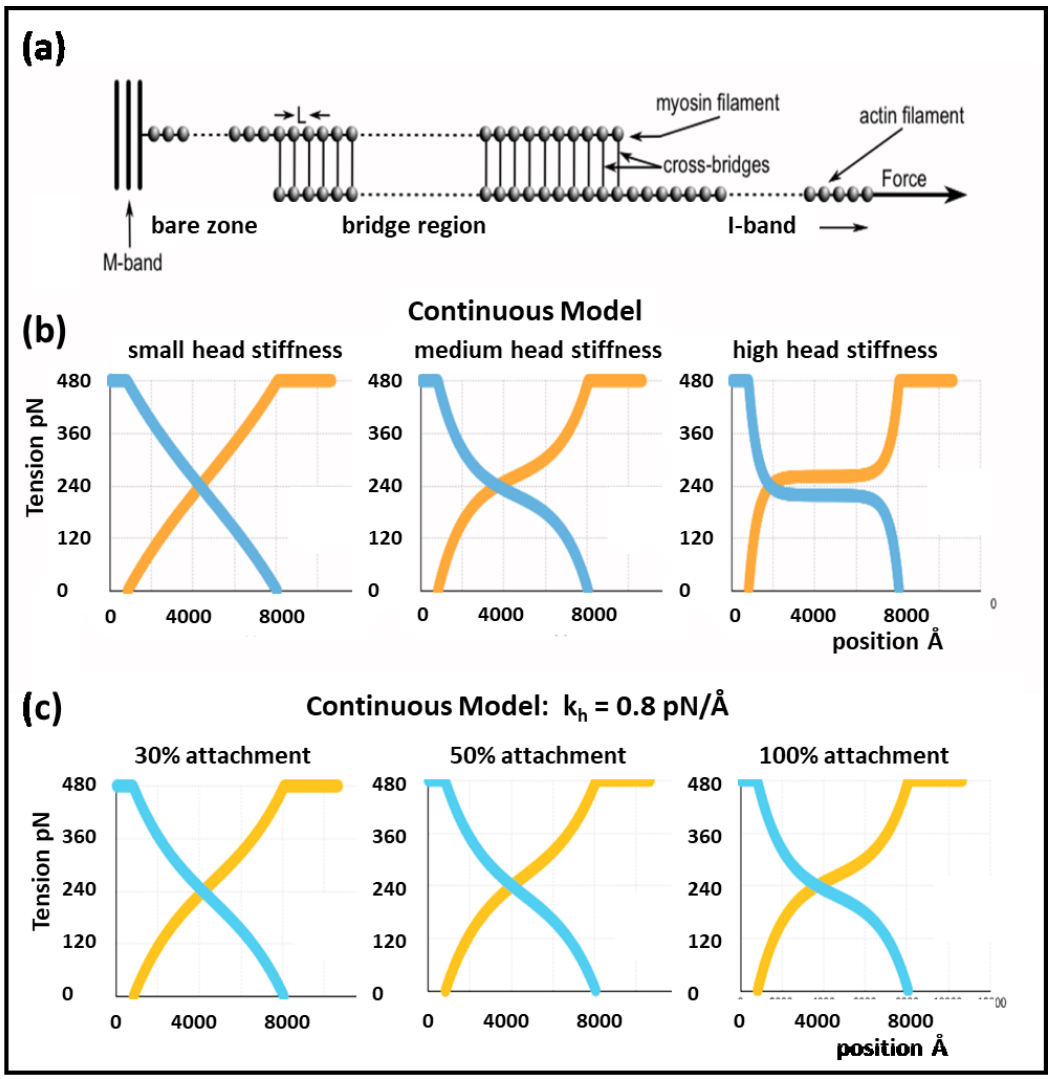

Figure 11: (a) A discrete Model that mimics the 'continuous' Model of Ford *et al* [4, 5]. For details see text. (b) Tension curves calculated using the Model in (a); left column - small head stiffness, k_h = 0.08 pN/Å; middle column - medium head stiffness, k_h = 0.8 pN/Å; right column - high head stiffness, k_h = 8 pN/Å. (c) As (b) but for varying attachment percentages with k_h = 0.8 pN/Å throughout. In all cases k_m = 720 pN/Å for the myosin filament, and k_a = 2280 pN/Å for the actin filament.

The shape of the tension curves depends on the value of the head stiffness and the percentage attachment (Figure 11(b,c)). As for Models 2 and 3, for small head stiffness values (K_h = 0.08 pN/Å; Figure 11(b)) the curves are almost linear. For medium values (K_m = 0.8 pN/Å) they deviate

noticeably from linearity, and for high values ($\mathbf{K_m}$ = 8 pN/Å) they are almost constant in the overlap region. The calculations described earlier using Model 1, 2 and 3 suggest values for the head stiffness in the medium range. Likewise the curves become more non-linear as the percentage attachment increases (Figure 11(c)). These results point to the fact that the basic assumption of tension linearity as in Figure 8(a) on which previous estimates of cross-bridge stiffness were been made were incorrect.

4.5 The myosin head stiffness: Implications about the cross-bridge cycle

Our modelling concludes that the apparent stiffness of the myosin heads in rapid length step experiments on frog (Rana temporaria) fibres at around 0-4°C is about $\mathbf{k_h}$ = 0.88 pN/Å for 30% attachment, assuming that all the parameters in the earlier list of observations are reasonably accurate. In particular this depends on using a T_1 cutoff of -40 Å as preferred by Ford *et al* [3,4]. We note that Linari *et al* [24] did the same experiment on a short fibre segment that would reduce errors and they too obtained a T_1 cutoff of around -40 Å. If this value is correct then, at the very least, from Figure 8, k_h appears to be larger than 0.4 pN/Å.

The energy available from the hydrolysis of one ATP molecule from ATP to ADP is about 60 - 70 kJ/mol under muscle conditions [28], which converts to about 50 pN.nm or 500 pN.Å available for work if the cross-bridge cycle is about 50% efficient. As discussed earlier, the average force generated per head in a fully active frog muscle producing 480 pN per half myosin filament with, say, 30% head attachment is:

F per head = 480 / (294 x 0.3) = 5.45 pN

If this force produces swinging of the lever arm of the myosin head, then the force will be at a maximum before the lever arm starts to swing and will then reduce to zero at the end of the swing, so we can say that the force goes from 10.9 pN at the start of the swing and drops to zero at the end of the swing to give the 5.45 pN average. If a force **F** moves an object by a distance **x** then the work done is **Fx**. Here **F** is on average 5.45 pN, the energy available is 500 pN Å, so **x** is 500/5.45 = 92 Å, a value that seems very consistent with results on the cross-bridge shapes in different states from protein crystallography [15]. For simplicity we will call this 100 Å.

Looking at this another way, we are assuming that when AM.ADP.Pi converts to AM.ADP and then to AM during force generation in an isometric muscle with no filament sliding, then the force so produced is taken up and stored by some sort of spring element in the cross-bridge. If this spring element is Hookean and of stiffness **k** and then delivers all its energy through a lever arm swing during filament sliding of 100 Å [15], then the stiffness of the spring would be given by:

Energy in stretched spring = 0.5 * **k** * $\mathbf{x}^2$ = 500 pN Å

So, if **x** is 100 Å, then **k** = 500/(0.5 * 100^2) = 0.1 pN/Å

But we find that the measured stiffness per cross-bridge in rapid shortening experiments is about 0.4 to 0.88 pN/Å; about 4 to 9 times as big. Putting our range of **k** = 0.4 to 0.88 pN/Å in the equation above gives a value for **x** of only 31.6 to 34 Å. This kind of observation is why some authors have proposed that the cycle must consist of multiple steps. But is that the only possibility? Below we present an alternative cross-bridge scenario that appears to fit the observations better.

4.6 The weak binding heads

As mentioned above, one of the discoveries of Bernhard Brenner and his colleagues (e.g. [27] and references therein) is that weak binding heads, heads carrying ADP and phosphate (i.e. M.ADP.Pi) in an otherwise relaxed muscle, provide a great deal of stiffness in muscles that are stretched very fast. There is a rapid equilibrium between M.ADP.Pi and (A)M.ADP.Pi. This was particularly apparent in rabbit muscle at low ionic strength where the weak binding population could be artificially enhanced. Because the heads are weak binding, in rapid equilibrium between attached and detached, the faster the applied stretch, the higher the stiffness reaches. Eventually, the stiffness should level off, if the stretch is fast enough, but Brenner *et al.* [27] were unable to reach this point. However, they did show that, for speeds of the order of 10^4 nm/hs/s, the weak binding head stiffness, at least in a pyrophosphate (PPi) solution, could be as high, or higher than, that of rigor heads under the same conditions.

Many recent studies of the cross-bridge cycle have concluded that weak binding heads are actually part of the normal contractile cycle. Eakins *et al*. [23] estimated that the weak binding/first attached population is about 20 % of the heads in a normal isometrically contracting fish muscle. Brenner *et al*. [27] estimated the weak binding population as about 10-20% in an active rabbit psoas fibre. Huxley and Kress [29] concluded, on the basis of the lack of change of the equatorial X-ray I_{11}/I_{10} intensity ratio in quick release or active shortening experiments, that there must be a substantial population of weak binding heads in active frog muscle. As discussed earlier, these studies also showed changes in the 11 equatorial X-ray diffraction peak well ahead of tension rise, indicating the attachment of non-force-producing (weakly-binding?) heads well before tension generation. It also seems evident that these weak binding heads in an active frog muscle fibre must contribute to the apparent stiffness of the fibre. Ford *et al*. [4] quote a shortening speed such that the step was complete in about 0.2 ms. Since we are dealing with step amplitudes up to and beyond 40 Å (i.e. 4 nm), their shortening speed of 4 nm in 0.2 ms was $2*10^4$ nm/hs/s; exactly the same sort of range as Brenner *et al*'s observation of rigor-like stiffness from weak binding heads in PPi. The PPi stiffness was observed to be higher than for heads in MgATP solutions, but, even so, rapid shortening of intact fibres must be sensing the stiffness of the weak binding heads, as well as any other attached heads.

Brenner *et al.* [27] showed that fibre stiffness in relaxed rabbit psoas fibres, at 20 mM ionic strength, undergoing length changes of $2*10^4$ nm/hs/s were about as stiff as rigor fibres (where the stiffness is relatively insensitive to the speed of stretch). The implication of their results is that, for even faster stretches or releases, the stiffness could be higher than that of rigor heads. The unknown in these experiments on relaxed muscle is the number of attached heads providing the stiffness. But the number of weak-binding heads is always going to be less than (possibly much less than – they only spend some of their time attached) or equal to the number of attached heads in rigor. In other words, weak binding heads in very fast length steps may appear even stiffer than rigor heads because, in the weak binding state, the muscle appears just as stiff as in rigor, but with fewer heads attached.

696 In the Ford *et al* [4] experiments on intact frog muscle fibres, the ionic strength was normal,
697 but, as discussed above, active muscles probably have up to 20% of the heads in the weak-binding
698 state. The X-ray diffraction estimates of 10 to 20% would refer to the weak binding heads that are
699 actually attached in any instant to actin. These heads will also appear stiff if the muscle is pulled
700 fast enough, but they will not be stiff at normal speeds of muscle shortening (Vmax about 1600
701 nm/hs/s [28]; 12.5 times slower). According to Brenner *et al.* [27], a speed reduction of 10x would
702 give a stiffness reduction of at least 10-fold, and probably a lot more.

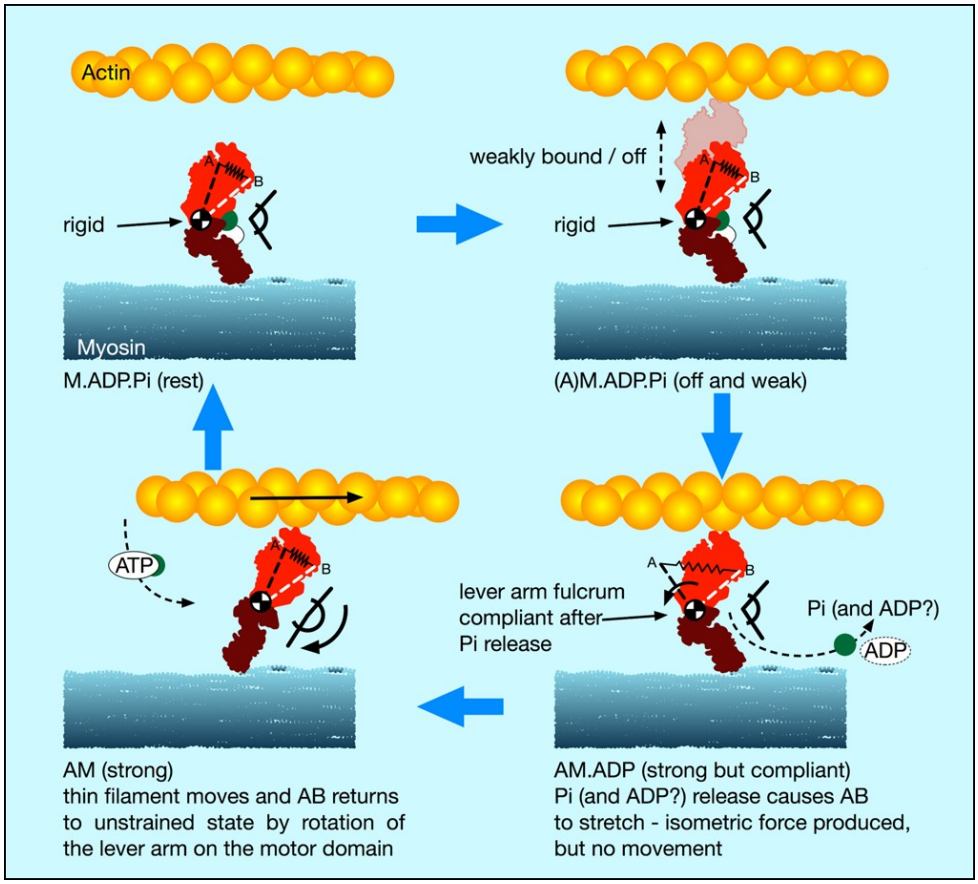

703

704 **Figure 12: The new cross-bridge scenario:** The spring AB represents the elastic state of the head. Top left:
705 Relaxed muscle with hydrolysis products ADP and Pi on myosin (M.ADP.Pi) has relatively rigid, but bent,
706 myosin heads with the fulcrum (converter domain?) between the motor domain and lever arm relatively stiff.
707 On activation (top right; (A)M.ADP.Pi), the heads go into a weak binding state on actin in which the heads are
708 still relatively rigid and these would make the muscle very stiff if it is stretched or released fast enough. Strong
709 binding to AM.ADP.Pi and release of Pi (bottom right) causes an associated release of the converter/ lever arm
710 to a relatively elastic state. The new head shape wants to be relatively straight as in the bottom left panel (rigor-
711 like), but the lever arm cannot move if the myosin and actin filaments cannot move (e.g. under a high load or
712 isometric). The lever arm remains in its original position, but it now exerts force (indicated here by the
713 stretched spring, AB). If the filaments are free to move, then the lever arm swings on the actin-attached motor
714 domain (bottom left) until at the end of its stroke it exerts zero force; AB is back to its original shorter length
715 and the head is relatively straight. Binding of another ATP to give AM.ATP (flexible) releases the head from
716 actin. Hydrolysis of ATP to ADP and Pi then occurs, and the heads revert to the rigid but bent M.ADP.Pi state
717 (top left).

718

4.7 A new scenario for myosin head behaviour in active muscle

In the light of our new stiffness results and this discussion of weakly-binding heads, our suggestion about the cross-bridge cycle (Figure 12) in active muscle is as follows:

(i) There is a substantial population of weak binding heads (10-20%) in actively force-producing isometric muscle. This is the population of heads actually attached to actin at any instant.

(ii) Under normal contraction conditions and shortening speeds, these heads contribute very little to the fibre stiffness, because they detach very rapidly as the muscle shortens and provide little stiffness.

(iii) If active muscles are subjected to stretches or releases which are very much faster than Vmax, then the weak binding heads will contribute substantially to fibre stiffness. We suggest that most of the cross-bridge contribution to the T_1 stiffness observed by Huxley and Simmons and their colleagues [2-4] comes from these weak binding heads. From Figure 7(a), if the weak-binding head attachment population is 20% and the T_1 intercept is -40 Å, for a P_o of 480 pN, then the stiffness of the weak-binding heads would be around 1.2 pN/Å.

(iv) We postulate that the weak binding heads are stiff because, in the M.ADP.Pi state, some part of the hinge between the lever arm and the motor domain is relatively rigid (Fig. 12 top panels).

(v) We suggest that the effect of strong binding and release of Pi [15] may be to release this part of the hinge (converter domain?) between the lever arm and motor domain so that the lever arm/converter domain is relatively free and the whole assembly can then act as a relatively compliant spring. Our suggestion is that the stiffness of this spring could be about 0.1 pN/Å as required to give a 100 Å step from an energy supply of 500 pN Å assuming 50% efficiency. Release of Pi and ADP makes the natural preferred position of the lever arm to be relatively straight as in Figure 12 bottom left panel. However, if the lever arm is constrained, as in an isometric muscle, so that the myosin and actin filaments cannot move, then the strained lever arm will remain in its original 'heads bent' position (Figure 10 bottom right panel) and the lever arm will exert tension on actin.

(vi) We suggest that the cross-bridge stiffness could remain at about 0.1 pN/Å in the strongly bound states through the whole of the lever arm swing if the filaments are free to move, including through the AM.ADP state towards the AM (rigor state; Fig. 10 bottom left panel).

(vii) The final rigor (AM) state is then slightly stiffer than the strong AM.ADP.Pi and AM.ADP states, at about 0.4 to 0.5 pN/Å under the conditions discussed here, but is relatively very short lived.

(viii) Binding of ATP, head release from actin, and the ATP hydrolysis step then return the heads to the M.ADP.Pi state in which the whole head is now relatively rigid again and the cycle can restart.

Note that, in this scenario, the strongly bound heads are clearly providing the observed tension and the tension reduction in the shortening step clearly means that, as well as the filaments shortening thus reducing tension, the lever arms of these strong heads would also be moving to reduce the tension in the cross-bridge spring element. At the same time the weakly bound heads will be resisting this shortening and will contribute the major part of the stiffness of the system. The relative contributions of the weak and strong heads to the observed stiffness will be in proportion to their individual stiffnesses, either 0.1 pN/Å for the strong heads (if our suggestion is

plausible) or greater than 0.4 pN/Å for the weak-binding heads. So, in this scenario, the T_1 behaviour will be dominated by the properties of the weak binding heads.

4.8 Implications of the mechanism

With this scenario, the stiffness in normal active muscle will not be affected much by the weak binding heads and the full cycle of one ATP turnover will be able to generate 100 Å of movement if the filaments are free to slide. However, if very fast mechanical steps are applied, then the weak binding head stiffness will come into play and the measured stiffness will depend on the speed of the step and may appear very large, even larger than in rigor if the applied steps are fast.

We suggest that an implication from this is that, in relaxed muscle, the myosin head domain is relatively rigid, which may help to explain why there is a relatively well-defined interacting heads motif in resting myosin filaments in the super-relaxed state [30-34]. The increased stiffness of the myofibril generated by the weak-binding heads when there are very rapid length changes, for example as a result of sudden mechanical shocks, may also be a safety mechanism to minimise structural damage to the sarcomere. The sarcomere will have a suddenly increased resistance to stretch that will alleviate any damaging effects of rapid internal length changes.

Are there other experimental observations which are consistent with this model? One of the obvious features of the model is that, if it is the weak binding heads that largely determine the T_1 cut-off, then the slope of the T_1 curve should depend on the speed of stretch or release. In fact, the observations of Ford *et al* [3], in their Figure 19, show recorded T_1 curves for steps complete in either 0.2 or 1 ms. The initial slopes of these two curves are, in fact, quite different, with the slope for a 1 ms step being significantly less steep (i.e. showing less stiffness) than that for the 0.2 ms step. This is exactly what would be expected if it is weak-binding heads that are being sensed. This result is emphasised even more by the summary analysis of Barclay *et al* [35] who showed T_1 plots from various authors from fibres shortened at 5 different speeds with steps complete in times ranging from 0.11 ms to 1.0 ms. Within experimental error, there is a systematic change in slope of the T_1 response as the speed changes, with lower stiffnesses (lower T_1 slopes) being observed at lower speeds.

Another observation by Colombini *et al* 2010 [36], Cecchi *et al*, 1982 [37]; Bagni *et al* (1999) [38] and references therein is that during the rising phase of tension generation, and under some other conditions, the measured stiffness changes much faster than the measured tension. This could possibly mean that the heads need to attach strongly first, in a strong pre-tensing step, giving stiffness but no tension, and then, after a delay, phosphate release and tension generation occur. Alternatively, with our model, this would be consistent with the suggestion that it is the weak-binding heads providing the early stiffness and the strong binding heads later providing the tension. Consistent with this, the X-ray observations of Martin-Fernandez *et al* [39], Harford and Squire [40], Eakins *et al* [23] and many others, show that the increase in the 11 equatorial X-ray reflection from contracting muscle, often taken to show actin-attachment of myosin heads and which is sensitive to the presence of weakly-binding heads [27], occurs well before tension generation.

Another well-known effect is that the tension in a fibre changes significantly if the temperature is changed or if, for example, in skinned fibres, the Pi or ADP concentrations are altered [41-45]. However, even though the tension changes, the stiffness of the fibres remains fairly constant. Since the tension changes are clearly due to the strongly attached heads, it is apparent that EITHER the changed temperature, or changed [ADP] or [Pi], alters the distribution of heads between strongly

attached states without the number of attached heads changing and they all have the same stiffness, hence keeping the total stiffness constant OR the stiffness is actually reporting something other than the strongly attached states that are producing the tension, in other words the weakly-bound heads. So there is evidence that is consistent with the idea that, apart from filament compliance, the T_1 curve is mainly reporting the properties of weakly-binding heads.

In a recent, sophisticated, mechanical study by Percario *et al* [46] they compared the mechanical properties of fast (psoas) and slow (soleus) muscles of the rabbit. They used Ca^{2+}-activation of permeabilised fibres and studied tension generation and stiffness in active fibres and stiffness in rigor fibres. They found for maximally-activated fibres (pCa 4.5) that the T_1 cutoff in steps complete in 0.11 ms at 12.2°C was around -50 Å for slow fibres (starting force about 150 kPa) and around -70 Å for fast fibres (starting force around 250 kPa). Starting from similar tension values as the active values in each case, the T_1 intercept for the rigor fibres was around 50 Å for both fast and slow fibres. What we know about rigor vertebrate muscle is that there is evidence that all the myosin heads are attached strongly to actin (Lovell *et al* [47], Cooke and Franks, 1980 [48]). In the two fibre types, the rigor stiffnesses stay the same for different starting tensions, in other words, in each case, the slopes of the T_1 curves remain the same even when they are shifted to different starting tensions. But the rigor T_1 slopes are different for the fast and slow fibres. The rigor T_1 curve is steeper for the fast fibres, meaning that the rigor cross-bridge stiffness is higher in the fast fibres. The main difference between the contractile machinery in the two fibre types is that there are two different myosin heavy chain types; the slow fibres have MHC-1 and the fast fibres MHC-2X. So these two myosin types appear to have different rigor stiffnesses. For active fibres, Percario *et al* [46] estimated that the maximal isometric force per myosin head is about 0.9 pN for slow fibres and about 1.6 pN for fast fibres.

So how do these results fit in with our new proposal for the crossbridge cycle with the weakly-binding head stiffness dominating the head part of the T_1 curve? If the lattice geometries in the fast and slow fibres are the same, and if the attachment number is 100% in both cases, then the different stiffnesses in the two rigor fibre types must mean that the myosin heads are intrinsically more compliant in slow fibres; MGC-1 heads must be more compliant than MHC-2X heads. This result may well apply to the same myosin head types in the weakly-binding states as well. In addition, when more myosin heads are recruited to give higher generated tensions, presumably the population of weakly-binding heads could increase too. These results would directly explain the less steep slope of the T_1 curve from slow fibres, if, apart from filament compliances, it is the weakly-binding heads which are mostly contributing to the slope of the T_1 curve.

In another recent study, Pinzauti *et al* [49] looked at the mechanical properties of cardiac muscle. They used rat trabeculae either electrically stimulated or skinned and put into rigor. They used steps complete in 0.11 to 0.13 ms, and a temperature of around 27°C. They found T_1 intercepts ranging from -40 to -70 Å depending on the Ca^{2+} concentration outside the trabeculae; 0.5 mM (-40 Å, T(tension) ~ 30kPa), 1.0 mM (-70 Å, T ~ 70 kPa), 2.5 mM (-80 Å, T ~ 100 kPa). So, the higher the external Ca^{2+} concentration, the higher was the tension, and the T_1 intercept was at ever larger negative values, with the T_1 slope gradually increasing. If the increased tension is due to the recruitment of more heads into the strong-binding states, then, as mentioned above, presumably the weakly-binding head population could also increase and the T_1 curve will get steeper, as observed.

So far we have said little about the possible effects of C-protein (MyBP-C [50]). C-protein labels the central one-third of the myosin filament bridge region in each half sarcomere [19], binds

specifically through its C-terminus to the myosin filament backbone [32], and can bind towards its N-terminus either to the myosin S2 [51] or to actin, or both. It is well-documented that in relaxed muscle C-protein can span the gap from the myosin filaments to the actin filaments (e.g. [52,53]). These results were firstly from vertebrate skeletal muscle, but cardiac C-protein also has additional regulatory effects through phosphorylation towards its N-terminal domains [54,55]. On activation of vertebrate skeletal muscle, a meridional X-ray reflection thought to be due to C-protein (at 442 Å) becomes much weaker well ahead of tension generation [39], an effect thought to indicate early detachment of C-protein from actin in active muscle and subsequent axial disorder. If C-protein was still attached to actin during contraction it could provide some of the observed T_1 stiffness, but, in view of the X-ray changes quoted above [39], continued C-protein attachment to actin in active muscle seems unlikely. However, the effects of transient attachment, which may also reduce the 442 Å peak cannot be ruled out.

5. Conclusion

Using our new, modified, MusLABEL program to model the known elasticities in the sarcomere with a sensible pattern of head labelling of actin, we have found that the head stiffness from the T_1 curve of Huxley and Simmons [2] is higher than has been estimated previously (> 0.4 pN/Å). We believe that this difference may be due to the fact that in most previous studies the tension through the myosin and actin filaments was assumed to vary linearly along their length in the overlap region of the half sarcomere. To quote Barclay *et al* [35], acknowledging the presence of filament compliance,: *'Consequently, fibre stiffness cannot be used as a direct index of the number of attached cross-bridges and* y_o (the T_1 intercept) *cannot be used as an index of the average strain of attached cross-bridges. However, if we know the average strain of structures other than attached cross-bridges at the moment a length step is applied* ***and if we assume strain depends linearly on force*** (our bold type), *then the proportion of the length step taken up by compliant structures in series with attached cross-bridges can be calculated and thus the length change that is transmitted to the cross-bridges can be found.'* And also '*For example, when the total force is T kPa, the force at the tip of the myosin filament is zero and only between the M-line and the end of the overlap region is the force on the filament equal to T. The average force in the overlap region is T/2.*'

However, our results (Figures 9 and 10) and direct model simulation of such previous approaches to take account of filament compliance (Figure 11) show that the tension is very non-linear through the overlap region. We are saying that filament strain does not depend linearly on the force at the filament ends in the overlap region. This applies to both myosin and actin filaments. This applies to both myosin and actin filaments and is the main difference between our analysis and what has gone before.

In addition, we suggest from analysis of various observations that much of the 'instantaneous' cross-bridge stiffness comes from the weak-binding head population in active muscle.

The results presented here, although suggesting many more experiments that might be used to test these ideas, also show that it is unlikely that the T_1 response can be used to determine the stiffness or occupancy of the strongly bound myosin head states. But it does seem inconceivable to us that the significant population of weakly-binding heads in active muscle does not contribute a significant part of the cross-bridge stiffness measured in the T_1 curve with the very fast step speeds used in the transient studies.

We suggest a possible cross-bridge cycle in Figure 12, with detached heads being stiffer than heads in strong states, which could explain directly how the myosin heads in isometric muscles can produce a stroke size of 100 Å from the energy of one turnover of ATP. It is a speculative idea open to be tested. However, there is no reason to believe *a priori* that all myosin head states must be equally stiff, and others have discussed non-linear cross-bridge compliance [12].

If our modified cross-bridge cycle is correct (Figure 12), then our enhanced MusLABEL program can be used to determine approximately the weak-binding cross-bridge stiffness or T_1 intercept at zero force for a given shortening speed if the M15, A13 or M3 position measurements are determined for a muscle with a known value of P_o at a known temperature and a known percentage attachment of weak-binding heads (perhaps modelled from X-ray observations [23]).

Acknowledgments: We are very much indebted to Dr. Gerald Offer and Professor K.W. Ranatunga for many stimulating discussions and for their detailed comments on the manuscript. JMS was supported by the European MYORES network and the British Heart Foundation during the initial stages of this work and is currently funded on BHF Fellowship grant to Dr. Danielle Paul (FS/14/18/3071).

Author Contributions: Conceptualization, Carlo Knupp and John M. Squire; Data curation, Carlo Knupp and John M. Squire; Formal analysis, Carlo Knupp and John M. Squire; Investigation, Carlo Knupp and John M. Squire; Methodology, Carlo Knupp and John M. Squire; Project administration, John M. Squire; Software, Carlo Knupp; Supervision, John M. Squire; Writing – original draft, John M. Squire; Writing – review & editing, Carlo Knupp and John M. Squire.

Conflicts of Interest: The authors declare no conflict of interest.

Appendix A: Model Calculations

In the vertebrate striated muscle sarcomere the unit cell contains one myosin filament and two non-equivalent actin filaments. Let us call this a contractile unit. Apart from any effects of the sarcoplasmic reticulum or connective tissue, which are unlikely to contribute significantly to the observed transient responses, modelling the elastic behaviour of one contractile unit is sufficient to model the whole half sarcomere, apart from considerations of possible small locally variable overlap changes. This is because if, say, we modelled ten contractile units instead of one, the stiffness would be ten times as large as for one contractile unit and we would need to divide the result by ten to get back to the behavior of one unit. We have not taken account of possible sarcomere length variations along a myofibril, which would make the computations impractical.

First we look at the calculations based on Model 2 in Figure 2(c). Looking at the balance of forces on each node (m_i or a_i) in the Figure, where m_i or a_i define the number and position of myosin crown i or actin repeat i and writing down the balance of forces (where $\Delta F = k\,\Delta x$; force change ΔF, elastic constant k and extension Δx).

For the myosin crowns (L ~ 145 Å):

$$-k_b(m_1 - B) + k_m(m_2 - m_1 - L) + k_h(a_1 - m_1) = 0$$

$$-k_m(m_2 - m_1 - L) + k_m(m_3 - m_2 - L) + k_h(a_2 - m_2) = 0$$

$$-k_m(m_3 - m_2 - L) + k_m(m_4 - m_3 - L) + k_h(a_3 - m_3) = 0$$

and so on to:

$$-k_m(m_y - m_{y-1} - L) + k_h(a_y - m_y) = 0$$

For the actin repeats also L long:

$-k_h(a_1 - m_1) + k_a(a_2 - a_1 - L) = 0$

$-k_h(a_2 - m_2) - k_a(a_2 - a_1 - L) + k_a(a_3 - a_2 - L) = 0$

$-k_h(a_3 - m_3) - k_a(a_3 - a_2 - L) + k_a(a_4 - a_3 - L) = 0$

and so on to:

$-k_i(a_{z-1} - a_z - I) + F = 0$

[F is applied force; elastic constants for bare zone, myosin filaments, actin filaments, myosin heads and I-band are k_b, k_m, k_a, k_h and k_i respectively. I-band length at start is I, bare zone length is B]

These equations can be rearranged:

e.g. $-k_b m_1 + k_b B + k_m m_2 - k_h m_1 - k_m L + k_h a_1 - k_h m_1 = 0$ etc.

and written down as a matrix which can be solved numerically using the Java library called JAMA: http://math.nist.gov/javanumerics/jama/. The results for Model 2 are shown in Figure 3.

In the case of Model 3 in Figure 2(d), similar equations can be set up as for Model 2, but they are now much more complicated. There are just over five actin monomers in a crown repeat, any of which could be labelled. Heads in a particular crown can attach to various actin monomers and two heads on the same crown can, for example, either attach to monomers at different axial positions in the same actin filament or to actin monomers in different actin filaments, but at the same or different axial positions. A summary of how the labelling is modelled in 3D using MusLABEL is given in Appendix B.

Appendix B: The 3D analysis involved in MusLABEL

MusLABEL [16] creates a parametric model of the thick filament and six surrounding thin filaments in half a sarcomere. A portion of this model, represented as a radial projection, is shown in Figure 13. After setting constraints for the azimuthal and axial movements of the myosin heads, along with the extent of the target regions on the thin filaments (as detailed in [16]), the best attachment sites of the myosin heads on actin (if available using the given parameters) are calculated. In the case of two or more attachment sites available for a given head, or in the case of two heads competing for the same site, the program pairs those heads and sites that minimise the overall elastic energy of the extending heads. Alternate thin filaments (depicted in white or light blue in the axial view in Figure 13(a) and the cross-sectional view in Figure 13(b)) are considered to be equivalent so that, if a head attaches to any actin monomer (red circle), the corresponding monomers on the other thin filaments (blue circles) become inaccessible.

To probe the elastic properties of the sarcomere, the three-dimensional model was projected to one dimension as a chain of myosin monomers flanked by two chains of actin monomers (Figure 13(c)). Of these chains, only the axial coordinates of each monomer along the main axis are considered for any subsequent calculation. Each chain representing the thin filaments is the 'sum' of all equivalent actins, on which all the head attachments are reproduced. Adjacent monomers in these chains are an axial distance **A** apart. The chain representing the thick filament was made of

equally spaced monomers an axial distance **L** apart. These correspond to the thick filament backbone monomers so that up to six separate heads can project outwards to attach to actin. Adjacent pairs of monomers in the actin and myosin chains are connected by elastic springs with spring constant $\mathbf{k_a}$ and $\mathbf{k_m}$ respectively. A force is applied to the terminal monomers of the actin chains towards the Z-line. The spring connecting the M-band to the myosin crown closest to the

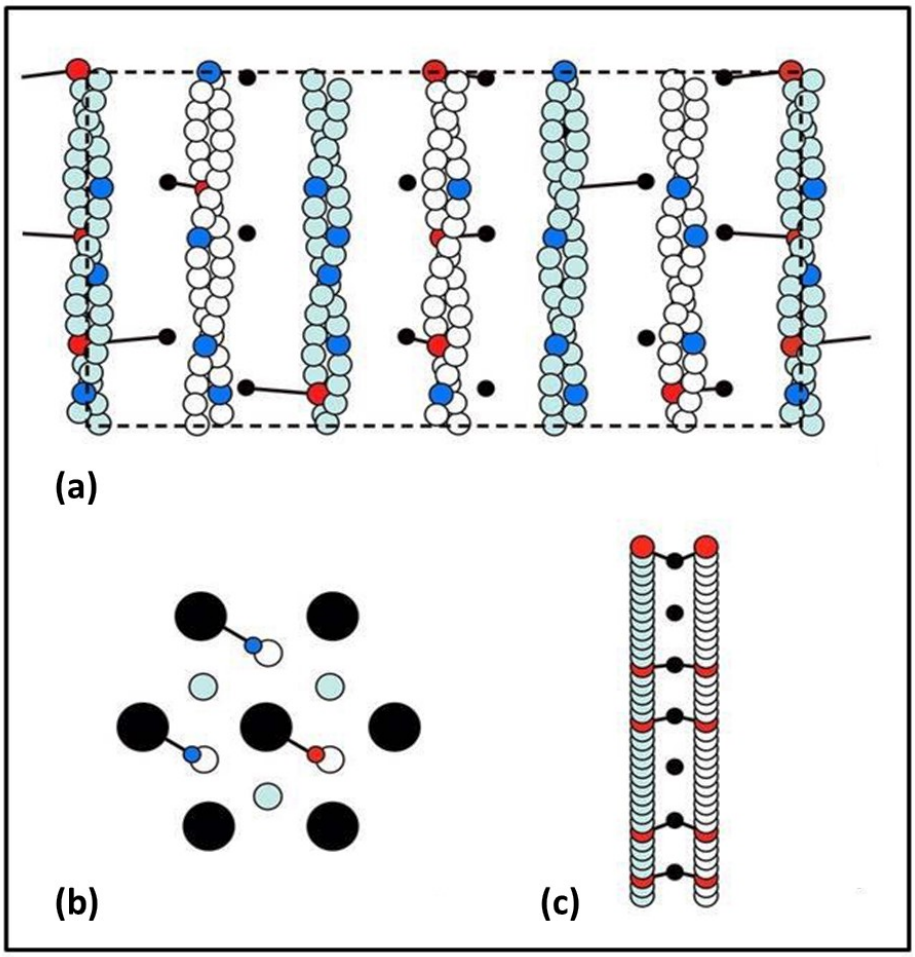

Figure 13: (a) Radial projection of a portion of the sarcomere's A-band. The myosin filament (represented by black circles at the resting positions of the myosin heads on the surface of the backbone) are surrounded by six actin filaments (the actin filaments on the far right and far left represent the same filament). The white actins are equivalent, and so are the light blue ones. The red circles represent actin monomers to which a head is attached. Blue circles represent inaccessible monomers on particular filaments, because a head is already attached there on an equivalent filament. (b) Cross-section of the sarcomere's A-band. A myosin filament (black circle in the middle) is surrounded by six other myosin filaments. In between there are actin filaments. Monomers with attached heads and equivalent filaments are colour coded as above. (c) One-dimensional Model obtained from (a). Black circles represent the myosin backbone and red circles the actin monomers with attached heads. Equivalent actin filaments have been merged together.

M-band (i.e. the half bare zone) is longer in size (with length **B**) and had spring constant $\mathbf{k_b}$. The M-band itself was kept fixed in space (Figure 2, Model 3). For simplicity a simple lattice A-band structure was assumed [18].

So the original MusLABEL analysis [16] was used to find which actin monomers were likely to be labelled by heads. To calculate the elastic properties of the system, with heads labelling these particular actin monomers, the same reasoning as in Appendix A was used, but with many more terms in the equations given there, in a modified version of MusLABEL. Each component of the system (i.e. myosin heads, actin monomers, myosin filament backbone etc) was then represented as a sphere with a variable size and weighting and the simulated meridional diffraction pattern was calculated using standard Fourier transform methods [14,25]. As detailed in the text, it was found that several combinations of parameters could explain the observed X-ray diffraction observations of Huxley *et al* [6] and Wakabayashi *et al* [7], so no definitive conclusions could be reached about cross-bridge behaviour from this X-ray modelling of the meridionals alone, except to say that the observations are easily explained (see example in Figure 4(a) and Table 1).

Appendix C: The various muscles and temperatures used.

We have analysed data from a number of sources, using a variety of muscle types and temperatures as shown in Table 2. Muscle type and temperature will both affect tension responses. We have shown in Figures 6 and 7 how this can be dealt with using our MusLABEL program.

Table 2: comparison of observed sources					
Reference	Ref No	Animal	Species	Muscle	Temperature
					(deg C)
Huxley and Simmons (1971)	2	frog	*Rana temPoraria*	semitendinosus	0 to 4
Ford *et al* (1977)	3	frog	*Rana temPoraria*	tibialis anterior	0 to 3
Ford *et al* (19081)	4	frog	*Rana temPoraria*	tibialis anterior	0 to 1
Huxley HE *et al* (1994)	5	bullfrog	*Rana catesbiana*	sartorius	10 to 14
				semitendinosus	10 to 14
Wakabayashi *et al* (1994)	6	bullfrog	*Rana catesbiana*	sartorius	8
				semitendinosus	8
Brenner *et al* (1986)	25	rabbit		psoas	5
Brunello *et al* (2014)	7	frog	*Rana esculenta*	sartorius	4
Eakins *et al* (2016)	21	fish	*Pleuronectes platessa* (plaice)	fin muscle	7 to 8

References

1. Huxley AF (1957) Muscle structure and theories of contraction. *Prog Biophys Biophys Chem* 7: 255-318.

2. Huxley AF, Simmons RM (1971) Proposed mechanism of force generation in striated muscle. *Nature* 233: 533-538.

3. Ford LE, Huxley AF, Simmons RM (1977) Tension responses to sudden length change in stimulated frog muscle fibres near slack length. *J Physiol*.269: 441-515.

4. Ford LE, Huxley AF, Simmons RM (1981) The relation between stiffness and filament overlap in stimulated frog muscle fibres. *J Physiol*. 311: 219-249.

5. Thorson J, White DCS (1969) Distributed representations for actin-myosin interactions in the oscillatory contraction of muscle. *Biophys J* 9: 360-390.

6. Huxley HE, Stewart A, Sosa H, Irving T. (1994) X-ray diffraction measurements of the extensibility of actin and myosin filaments in contracting muscle. *Biophys J*. ;67: 2411-2421.

7. Wakabayashi K, Sugimoto Y, Tanaka H, Ueno Y, Takezawa Y, Amemiya Y. (1994) X-ray diffraction evidence for the extensibility of actin and myosin filaments during muscle contraction. *Biophys J*. 67: 2422-2435. Erratum in: *Biophys J* 1995 68:1196-1197.

8. Brunello E, Caremani M, Melli L, Linari M, Fernandez-Martinez M, Narayanan T, Irving M, Piazzesi G, Lombardi V, Reconditi M. (2014) The contributions of filaments and cross-bridges to sarcomere compliance in skeletal muscle. *J Physiol*. 592: 3881-3899.

9. Offer G, Ranatunga KW. (2010) Cross-bridge and filament compliance in muscle: implications for tension generation and lever arm swing. *J Muscle Res Cell Motil*. 31: 245-265.

10. Mansson A, Usaj M, Moretto L, Rassier DE (2018) Do actomyosin single molecule mechanics data predict mechanics of contracting muscle? *Int. J. Mol. Sci.* 19, 1863; doi:10.3390/ijms19071863x.

11. Kaya M, Higuchi H (2013) Stiffness, working stroke and force of single myosin molecules in skeletal muscle: Elucidation of these mechanical properties via non-linear elasticity evaluation. Cell Mol Life Sci 70: 4275-4292.

12. Månsson A. (2010) Significant impact on muscle mechanics of small nonlinearities in myofilament elasticity. *Biophys J*. 99: 1869-1875.

13. Huxley AF, Tideswell S (1996) Filament compliance and tension transients in muscle. *J Muscle Res Cell Motil*. 17: 507-511.

14. Knupp C, Offer GW, Ranatunga KW, Squire JM (2009) Probing muscle myosin motor action: X-ray (m3 and m6) interference measurements report motor domain not lever arm movement. J Mol Biol. 390: 168-181.

15. Houdusse A, Sweeney HL. (2016) How Myosin Generates Force on Actin Filaments. Trends Biochem Sci. 41: 989-997.

16. Squire, J.M. & Knupp, C. (2004) MusLABEL: A Program to model Striated Muscle A-Band Lattices, to Explore Cross-bridge Interaction Geometries and to Simulate Muscle Diffraction Patterns. *J. Mus. Res. Cell Motil.* 25, 423-438.

17. Huxley, H.E. & Brown, W. (1967) The low-angle X-ray diagram of vertebrate striated muscle and its behaviour during contraction and rigor. *J. Mol. Biol.* **30**, 383-434.

18. Harford, J.J. and Squire, J.M. (1986) The 'crystalline' myosin cross-bridge array in relaxed bony fish muscles. *Biophys. J.* 50, 145-155.

19. Sjöström M, Squire JM. (1977) Fine structure of the A-band in cryo-sections. The structure of the A-band of human skeletal muscle fibres from ultra-thin cryo-sections negatively stained. *J Mol Biol*. 109: 49-68.

20. Squire JM (2009) Muscle myosin filaments: cores, crowns and couplings. *Biophys Rev*. 1: 149. doi: 10.1007/s12551-009-0017-4.

21. Elliott GF, Lowy J, Worthington CR (1963) An X-ray and light diffraction study of the filament lattice of striated muscle in the living state and in rigor. *J Mol Biol* 6: 295-305.

22. Knupp C, Luther PK, Squire JM (2002) Titin Organisation and the 3D architecture of the Vertebrate Striated Muscle I-Band. *J Mol Biol* 322: 731-739.

23. Eakins F, Pinali C, Gleeson A, Knupp C, Squire JM. (2016) X-ray Diffraction Evidence for Low Force Actin-Attached and Rigor-Like Cross-bridges in the Contractile Cycle. *Biology* 5. pii: E41. PMID: 27792170

24. Linari M, Dobbie I, Reconditi M, Koubassova N, Irving M, Piazzesi G, Lombardi V. (1998) The stiffness of skeletal muscle in isometric contraction and rigor: the fraction of myosin heads bound to actin. *Biophys J*. 74: 2459-2473.

25. Squire JM, Knupp C (2017) Studies of muscle contraction using X-ray diffraction. In '*Muscle Contraction and Cell Motility*' Ed H Sugi. pp.35-73.

26. Huxley AF (1974) Muscular contraction. *J Physiol*. 243: 1-43.

27. Brenner B, Chalovich JM, Greene LE, Eisenberg E, Schoenberg M. (1986) Stiffness of skinned rabbit psoas fibers in MgATP and MgPPi solution. *Biophys J*. 50: 685-691.

28. Barclay CJ. (2015) Energetics of contraction. *Compr Physiol*. 5: 961-995.

29. Huxley HE, Kress M. (1985) Cross-bridge behaviour during muscle contraction. *J Muscle Res Cell Motil*. 6: 153-161.

30. Wendt, T., Taylor, D., Messier, T., Trybus, K.M. & Taylor, K.A. (1999) Visualization of head-head interactions in the inhibited state of smooth muscle myosin. *J. Cell Biol*. 147, 1385-1390.

31. Woodhead JL, Zhao FQ, Craig R, Egelman EH, Alamo L, Padrón R. (2005) Atomic model of a myosin filament in the relaxed state. *Nature* 436: 1195-1199.

32. Al-Khayat HA, Kensler RW, Squire JM, Marston SB, Morris EP. (2013) Atomic model of the human cardiac muscle myosin filament. *Proc Natl Acad Sci U S A*. 110: 318-323.

33. Hu Z, Taylor DW, Reedy MK, Edwards RJ, Taylor KA (2016) Structure of myosin filaments from relaxed *Lethocerus* flight muscle by cryo-EM at 6 Å resolution. *Sci Adv*. 2: e1600058. eCollection PMID: 27704041.

34. Nogara L, Naber N, Pate E, Canton M, Reggiani C, Cooke R. (2016) Spectroscopic Studies of the Super Relaxed State of Skeletal Muscle. *PLoS One*. 11: e0160100. doi: 10.1371/journal.pone.0160100.

35. Barclay CJ, Woledge RC, Curtin NA (2010) Inferring cross-bridge properties from skeletal muscle energetics. *Prog Biophys. Mol Biol* 102: 53-71.

36. Colombini B, Nocella M, Bagni MA, Griffiths PJ, Cecchi G (2010). Is the cross-bridge stiffness proportional to tension during muscle fiber activation? *Biophys J* 98: 2582–2590.

37. Cecchi G, Griffiths PJ, Taylor S (1982) Muscular contraction: Kinetics of croissbri9dge attachment stufied by high-frequency stiffness measurements. *Science* 217: 70-72.

38. Bagni MA, Cecchi G, Colombini B, Colomo F (1999) Sarcomere tension-stiffness relation during the tetanus rise in single frog muscle fibres. *J Mus Res Cell Motil* 20, 469-476.

39. Martin-Fernandez ML, Bordas J, Diakun G, Harries J, Lowy J, Mant GR, Svensson A, Towns-Andrews E. (1994) Time-resolved X-ray diffraction studies of myosin head movements in live frog sartorius muscle during isometric and isotonic contractions. *J Muscle Res Cell Motil* 15: 319-348.

40. Harford JJ, Squire JM (1992) Evidence for structurally different attached states of myosin crossbridges on actin during contraction of fish muscle. Biophys J 63: 387-396.

41. Galler S, Hilber K (1998) Tension/stiffness ratio of skinned rat skeletal muscle fibre types at various temperatures. *Acta Physiol Scand* 162:119-126.

42. Decostre V, Bianco P, Lombardi V, Piazzesi G (2005) Effect of temperature on the working stroke of muscle myosin. *Proc Natl Acad Sci USA* 102: 13927-13932.

43. Coupland ME, Pinniger GJ, Ranatunga KW (2005) Endothermic force generation, temperature-jump experiments and effects of increased [MgADP] in rabbit psoas muscle fibres. *J Physiol* 567: 471-492.

44. Ranatunga KW, Coupland ME, Mutungi G (2002) An asymmetry in the phosphate dependence of tension transients induced by length perturbation in mammalian (rabbit psoas) muscle fibres. *J Physiol* 542:899-910.

45. Linari M, Caremani M, Piperio C, Brandt P, Lombardi V (2007) Stiffness and fraction of myosin motors responsible for active force in permeabilized muscle fibres from rabbit psoas. *Biophys J* 92: 2476-2480.

46. Percario V, Boncompagni S, Protasi F, Pertici I, Pinzauti F, Caremari M (2018) Mechanical parameters of the molecular myosin II determined in permeabilised fibres from slow and fast skeletal muscles of the rabbit. *J Physiol* 596: 1243-1257.

47. Lovell SJ, Knight PJ, Harrington WF (1981) Fraction of myosin heads bound to thin filaments in rigor fibrils from insect flight and vertebrate muscle. *Nature* 293:664–666.

48. Cooke R, Franks K (1980). All myosin heads form bonds with actin in rigor rabbit skeletal muscle. *Biochem* 19: 2265–2269.

49. Pinzauti F, Pertici I, Reconditi M, Narayanan T, Steinen GJM, Piazzesi G, Lombardi V, Linari M, Caremari M (2018) The force and stiffness of myosin motors in the isometric twitch of a cardiac trabecula and the effect of the extracellular calcium concentration. *J Physiol* 596: 2581-2596.

50. Offer G, Moos C, Starr R (1973) A new protein of the thick filaments of vertebrate skeletal myofibrils. Extractions, purification and characterization. *J Mol Biol* 74:653–676

51. Gruen M, Gautel M (1999) Mutations in beta-myosin S2 that cause familial hypertrophic cardiomyopathy (FHC) abolish the interaction with the regulatory domain of myosin binding protein-C. *J Mol Biol* 286: 933–949

52. Luther PK, Winkler H, Taylor K, Zoghbi ME, Craig R, Padron R, Squire JM, Liu J (2011) Direct visualization of myosin-binding protein C bridging myosin and actin filaments in intact muscle. *Proc Natl Acad Sci USA* 108:11423–11428.

53. Squire JM, Luther PK, Knupp C (2003) Structural evidence for the interaction of C-protein (MyBP-C) with actin and sequence identification of a possible actin-binding domain. *J Mol Biol* 331:713–724

54. Gautel M, Zuffardi O, Freiburg A, Labeit S (1995) Phosphorylation switches specific for the cardiac isoform of myosin binding protein-C: a modulator of cardiac contraction? *EMBO J* 14: 1952–1960.

55. Pfuhl M, Gautel M (2012) Structure, interactions and function of the N-terminus of cardiac myosin binding protein C (MyBP-C): who does what, with what, and to whom? *J Mus Res Cell Motil* 33: 83-94.

56. Kensler RW, Craig R, Moss RL (2017) Phosphorylation of cardiac myosin binding protein C releases myosin heads from the surface of cardiac thick filaments. *Proc Natl Acad Sci USA* 114: E13255-E1364.